HHS Public Access

Author manuscript

Cancer Discov. Author manuscript; available in PMC 2023 February 05.

Published in final edited form as:

Cancer Discov. 2022 August 05; 12(8): 1960–1983. doi:10.1158/2159-8290.CD-20-1628.

Interleukin-27 signaling serves as an immunological checkpoint for innate cytotoxic cells to promote hepatocellular carcinoma

Turan Aghayev[1,#], **Aleksandra M. Mazitova**[1,2,#], **Jennifer R. Fang**[3,#], **Iuliia O. Peshkova**[1], **Matthew Rausch**[4], **Manhsin Hung**[5,6], **Kerry F. White**[4], **Ricard Masia**[4], **Elizaveta K. Titerina**[1], **Aliia R. Fatkhullina**[1], **Isabelle Cousineau**[7], **Simon Turcotte**[7], **Dmitry Zhigarev**[1], **Anastasiia Marchenko**[2], **Svetlana Khoziainova**[2], **Petr Makhov**[8], **Yin Fei Tan**[9], **Andrew V. Kossenkov**[10], **David L. Wiest**[1], **John Stagg**[7], **Xin Wei Wang**[5,6], **Kerry S. Campbell**[1], **Amiran K. Dzutsev**[3], **Giorgio Trinchieri**[3], **Jonathan A. Hill**[4], **Sergei I. Grivennikov**[2,11,*], **Ekaterina K. Koltsova**[1,2,12,*]

[1]Blood Cell Development and Function Program, Fox Chase Cancer Center, Philadelphia, PA 19111, USA

[2]Cedars-Sinai Medical Center, Cedars-Sinai Cancer Institute, Department of Medicine, Department of Biomedical Sciences 8700 Beverly Blvd, Los Angeles, CA, 900048

[3]Laboratory of Integrative Cancer Immunology, Center for Cancer Research, National Cancer Institute, National Institutes of Health, Bethesda, MD, USA, 20892

[4]Surface Oncology Inc., 50 Hampshire St. Cambridge, MA, 02139

[5]Laboratory of Human Carcinogenesis, Center for Cancer Research, National Cancer Institute, National Institutes of Health, Bethesda, MD, USA, 20892

[6]Liver Cancer Program, Center for Cancer Research, National Cancer Institute, National Institutes of Health, Bethesda, MD, USA, 20892

[7]Centre Hospitalier de l'Université de Montréal Research Center, Montreal, Quebec, Canada

[8]Molecular Therapeutics Program, Fox Chase Cancer Center, Philadelphia, PA, 19111, USA

[9]Genomics Facility, Fox Chase Cancer Center, Philadelphia, PA 19111, USA

[10]Bioinformatics Facility, The Wistar Institute, Philadelphia, PA 19104, USA

[11]Cancer Prevention and Control Program, Fox Chase Cancer Center, Philadelphia, PA, 19111, USA

[12]Corresponding and Lead Author, contact: Ekaterina Koltsova, MD, PhD, Department of Medicine, Department of Biomedical Sciences, Cedars-Sinai Medical Center, 8700 Beverly Blvd, Los Angeles, CA, 900048, USA., phone: +1-310-423-8899, Ekaterina.Koltsova@cshs.org.

[#]these first authors equally contributed to this work

[*]these senior authors equally contributed to this work

Authorship Contributions

T.A., A.M.M., I.O.P., S.I.G and E.K.K. designed the study, planned the experiments and analyzed the data. T.A., I.O.P., A.M.M., E.K.T, A.F.R, D.Z., N.K., A.M., S. K., P.M., D.W., E.K.K. performed the experiments. K.F.W., M.R., and J.A.H. designed and performed experiments characterizing the activity of SRF381. R.M. performed histopathology analysis, J.R.F., A.D. and G.T. analyzed scRNAseq data, I.C., S.T., J.S., M.H. and X.W.W. performed the analysis of human cohorts, Y.F.T. assisted with scRNAseq, A.K. performed bioinformatic analysis of TCGA data. T.A., A.M.M., K.S.C., S.I.G., and E.K.K. wrote the manuscript with the input of other co-authors.

Abstract

While inflammatory mechanisms driving hepatocellular carcinoma (HCC) had been proposed, the regulators of anti-cancer immunity in HCC remain poorly understood. We found that IL-27 receptor (IL-27R) signaling promotes HCC development *in vivo*. High IL-27EBI3 cytokine or IL-27RA expression correlated with poor prognosis for patients with HCC. Loss of IL-27R suppressed HCC *in vivo* in two different models of hepatocarcinogenesis. Mechanistically, IL-27R signaling within the tumor microenvironment restrains the cytotoxicity of innate cytotoxic lymphocytes. IL-27R ablation enhanced their accumulation and activation, while depletion or functional impairment of innate cytotoxic cells abrogated the effect of IL-27R disruption. Pharmacological neutralization of IL-27 signaling increased infiltration of innate cytotoxic lymphocytes with upregulated cytotoxic molecules and reduced HCC development. Our data reveal an unexpected role of IL-27R signaling as an immunological checkpoint regulating innate cytotoxic lymphocytes and promoting HCC of different etiologies, thus indicating a therapeutic potential for IL-27 pathway blockade in HCC.

Introduction

Hepatocellular carcinoma (HCC) is the most common form of liver cancer with a poor survival rate and limited treatment options(1,2). While innovative therapeutic strategies targeting the tumor microenvironment and immune contexture provide hope to many cancer patients (3,4), HCC remains poorly responsive to therapies and continue to be a highly lethal disease (2,5). For example, despite wide clinical use of T cell activation-based immunotherapies in several cancer types (6), checkpoint inhibitors have only recently demonstrated potentially promising results in HCC (7). Preventive approaches aimed at hepatitis B vaccination and hepatitis C eradication could potentially curb new HCC cases, but liver cancers caused by environmental toxins and fatty liver disease are clearly on the rise (8,9).

Chronic liver inflammation induced by infections, alcohol or obesity drives chronic injury and promotes compensatory proliferation of transformed hepatocytes facilitating HCC formation and growth (10). While anti-cancer immune responses generally play an important tumor-restrictive role, it remains to be determined how they are regulated by the inflammatory entities in HCC (11).

Irrespective of its etiology, HCC development is accompanied by the accumulation of immune cells, which contribute to cancer progression via the production of pro-inflammatory cytokines such as Interleukin (IL)-6, IL-1, tumor necrosis factor (TNF) and IL-17 (12). Cytokine signaling enables HCC growth by activating proto-oncogenic transcription factors such as NF-κB and STAT3 in transformed hepatocytes and HCC cells (10,12–14). Conversely, the presence of cytotoxic or IFNγ-producing T cells suppresses tumor growth (15). Moreover, the liver microenvironment is uniquely enriched in innate lymphocytes including natural killer (NK) cells and innate lymphoid cells type 1 (ILC1), capable of tissue immunosurveillance and anti-tumorigenic functions potentially impacting HCC tumorigenesis (16,17). During HCC development, the number and activation state of liver NK cells gradually declines due to yet unidentified mechanisms possibly related to

specific signals originating from the cancer cells and the tumor microenvironment (18). The mechanisms that drive functional suppression of NK cells and hence undermine important innate anti-cancer immune responses remain incompletely understood.

IL-27 is a member of the IL-6/IL-12 cytokine superfamily and is an important regulator of immune responses (19). IL-27 is composed of two subunits, IL-27p28 and IL-27EBI3. The IL-27 receptor (IL-27R), composed of two chains, WSX-1/IL-27RA and gp130, is expressed by multiple immune cell subsets, including NK cells, and by some non-hematopoietic cells (20). IL-27R transmits signals primarily via STAT1 and STAT3 activation (19), amongst which STAT3 is a hepatocyte-intrinsic driver of HCC (21). IL-27 was shown to have a broad anti-inflammatory role in infectious and chronic immune-mediated diseases (22–24). IL-27RA ablation leads to elevated production of pro-inflammatory cytokines, including IL-17A and IL-6 (23,25), indicating that in inflammation-driven cancer, such as HCC, IL-27 could potentially play a tumor-restrictive, anti-inflammatory role. *In vitro* and *in vivo* experiments revealed that IL-27 enhances LAG-3, TIM-3, PD-1 and TIGIT inhibitory molecule expression in T cells (26). While immunomodulatory effects of IL-27 were shown in various pathophysiological models (27–31), the context-dependent and cell type-specific underlying mechanisms remain incompletely understood. The protective role of IL-27 and its receptor signaling in cancer has been suggested based on its anti-inflammatory role in inflammatory diseases and studies using subcutaneous cell line transplants (32–34) or spontaneous cancer development in a context of p53 deficiency (35), nevertheless the role of IL-27R signaling in cancer development *in vivo* has not been comprehensively addressed.

Here we found that genetic loss of *Il27ra* surprisingly suppressed liver cancer development in two different faithful *in vivo* models of HCC: diethylnitrosamine (DEN) carcinogen-driven and non-alcoholic steatohepatitis (NASH)-driven HCC. Analysis of several independent human HCC cohorts revealed that expression of *IL27RA* or increased serum protein levels of the IL-27 cytokine subunit EBI3 are associated with poor survival and enriched in patients with a more advanced stage of disease. Mechanistically, we found that IL-27R signaling limited the accumulation and activation of innate cytotoxic cells (NK and ILC1) in tumors, and *Il27ra* genetic ablation relieved the inhibition and resulted in infiltration of more activated cells that correlated with reduced HCC burden. Moreover, IL-27R signaling repressed expression of NK cell-activating stress ligands on tumor cells. Inactivation of IL-27R signaling in turn relieved this suppressive effect, most notably in bona fide cytotoxic NK cell populations and “cytotoxic-like” ILC1 populations, and enhanced cytotoxic anti-tumor immune responses *in vivo*. The dependence of IL-27R signaling driven immunoregulatory effects in HCC on innate cytotoxic cells was further established by $NK1.1^+$ cell depletion, which reverted the effect of IL-27R inactivation on HCC. Both IL-27 cytokine and IL-27R were amenable to pharmacological blockade resulting in reduced HCC, associated with heightened $NK1.1^+TCR\beta^-$ cell accumulation and upregulation of cytotoxic molecules, establishing the importance of this ligand-receptor pair in HCC biology and providing a rationale for their therapeutic neutralization. Taken together, our data suggest that inactivation of IL-27R signaling enhances innate cytotoxic cell cytotoxicity, providing new therapeutic opportunities in liver cancer as well as preventive approaches in high-risk patients with NASH and liver fibrosis who are likely to progress to HCC.

Results

IL-27/IL-27R axis is associated with poor prognosis in human HCC

While the role of IL-27R signaling has been investigated in infectious and inflammatory diseases (36–40), unequivocal evidence about its possible contribution to tumor development *in vivo* is missing. We assessed the protein levels of IL-27 cytokine in human serum, and found that IL-27EBI3 subunit was significantly elevated in patients with HCC compared to healthy controls (Fig. 1A). These increased levels of IL-27EBI3 were similarly observed in Hepatitis B or C virus positive or negative patients; and were independent of alpha-fetoprotein (AFP) levels (Supplementary Fig. S1A,B). Moreover, the probability of survival negatively correlated with the serum level of IL-27EBI3, where patients within the highest tertile group of IL-27EBI3 protein demonstrated the poorest overall survival while patients within the lowest tercile showed the best overall survival (Fig. 1B). Next, we evaluated the impact of *IL27RA* receptor expression in human HCC tumors on disease-free survival using TCGA data. Patients with high *IL27RA* expression exhibited poor disease-free survival and presented with more advanced stages of HCC (Fig. 1C, D). We also obtained similar results in previously described independent “SNU” (41) and “LCI” (42) HCC cohorts (Fig. 1E–G). These correlative expression data in human HCC samples may suggest potentially cancer-promoting role of IL-27R signaling in HCC. Such role was nevertheless surprising as active IL-27R signaling was previously shown to reduce the expression of IL-6, IL-17A and other inflammatory cytokines deemed pro-tumorigenic in HCC (12,23). The analysis of a published single cell RNA sequencing (scRNAseq) dataset of $CD45^+$ cells from human HCC (43) revealed that *IL27RA* is expressed by most of the tumor infiltrating immune cells, while *IL27EBI3* and *IL27P28* expression is mostly restricted to myeloid lineages (Fig. 1H–J). Similarly, IHC staining showed that at protein level, IL-27RA was expressed by infiltrating immune cells as well as cancer cells in human HCC tumors (Supplementary Fig. S1C).

IL-27R signaling promotes HCC development in DEN-induced model

To directly evaluate the role of IL-27R signaling in HCC we used a genetic approach in the well-established mouse model of HCC driven by the carcinogen DEN (10,44,45). To exclude the potentially confounding influence of microbiota, we used cage-mate and littermate controls. Male $Il27ra^{+/-}$ or $Il27ra^{-/-}$ mice were injected with 25 mg/kg of DEN i.p. at day 15 after birth, and tumor development was assessed at 10 months of age. We found that HCC tumorigenesis was markedly reduced in $Il27ra^{-/-}$ mice compared to $Il27ra^{+/-}$ controls (Fig. 1K, L), supporting the results from human cohorts. Body weight of tumor-bearing mice was not affected by *Il27ra* deficiency (Supplementary Fig. S1D). Serum level of ALT (alanine transaminase), a marker of liver damage reflecting HCC formation, was significantly lower in $Il27ra^{-/-}$ mice compared to their $Il27ra^{+/-}$ tumor-bearing counterparts, suggesting preserved liver function in the absence of IL-27R (Fig. 1M). No difference was detected in serum levels of albumin, globulin or total bilirubin (Supplementary Fig. S1E). Consistent with the limited tumor burden, HCC tumors from *Il27ra* deficient mice were also characterized by lower expression of the inflammatory marker lipocalin-2 (*Lcn2)* (Fig. 1N), proliferation markers Ki67 (Fig. 1O) and cyclin D1 (*Ccnd1)* (Fig. 1P), and reduced activation of kinase ERK1/2 (Supplementary Fig. S1F).

No difference in fibrosis was detected between genotypes (Fig. 1Q and Supplementary Fig. S1G), likely reflecting the inflammation-driven nature of the DEN model being less dependent on fibrosis (46). To determine if limited proliferation is a broader representation of IL-27R-dependent liver regenerative capacity, we compared liver regeneration in *Il27ra* deficient and sufficient mice. Partial hepatectomy of 2/3 of liver tissue revealed no significant differences between *Il27ra*$^{-/-}$ or control *Il27ra*$^{+/-}$ mice in the ability to regenerate liver mass (Supplementary Fig. S2A). Stimulation of HCC cells derived from DEN tumors with recombinant IL-27 (rIL-27) or shRNA knockdown of *Il27ra* did not affect cell growth *in vitro* as demonstrated by clonogenic assay (Supplementary Fig. S2B–D), despite IL-27 mediated induction of STAT3 phosphorylation in HCC cells (Supplementary Fig. S2E). These data suggest that IL-27R likely regulates HCC development independent of its effects on liver regeneration or cell autonomous effects on hepatocyte and cancer cells.

To further assess the contribution of IL-27R signaling to HCC in cancer versus immune and stromal cells, we first orthotopically implanted DEN-derived HCC cells with knockdown of *Il27ra* or control into the liver of *Il27ra* sufficient mice. The lack of IL-27R on tumor cells in the context of IL-27R sufficient immune environment did not affect tumor growth (Supplementary Fig. S2F,G). Conversely, we transplanted *Il27ra* sufficient HCC cells into the livers of *Il27ra*$^{-/-}$ or control mice and observed a substantial reduction of tumor growth in *Il27ra*$^{-/-}$ mice (Supplementary Fig. S2H, I). Collectively, our data demonstrates that IL-27R signaling in the microenvironment promotes HCC in DEN carcinogen-induced model *in vivo*.

IL-27R signaling restricts NK cell accumulation in HCC

HCC progression is regulated by various immune cells, accumulating in tumor and non-tumor tissue(12). In order to elucidate potential mechanisms by which IL-27R signaling controls HCC, we first conducted gene expression analysis on isolated DEN-induced HCC tumors from *Il27ra* deficient and sufficient animals. Among the most notable changes, we found an increase in natural killer (NK) cell-specific markers and overall upregulation of the NK-mediated cytotoxicity pathway in tumors of *Il27ra*$^{-/-}$ mice (Fig. 2A). We also found the enrichment in NK cell signature genes to be the highest among other immune cell signatures in the absence of IL-27R (Fig. 2B,C). Moreover, we found an upregulation of IL-15, a cytokine driving NK cell differentiation towards more mature, activated state (47,48), that was especially pronounced in tumors of *Il27ra*$^{-/-}$ mice (Fig. 2D), suggesting a potential role of IL-27R signaling in the control of NK cells in HCC. Flow cytometry analysis of immune cell composition in tumor and adjacent non-tumor tissue did not reveal any significant differences in numbers of CD8 or CD4 T cells, monocytes or neutrophils (the latter collectively representing the intratumoral MDSC population) in tumors, while we detected an increased presence of neutrophils in non-tumor tissues and reduction of macrophages in tumors of *Il27ra*$^{-/-}$ mice (Supplementary Fig. S3A–C). In agreement with the data obtained in mRNA gene expression analyses, we found a significant increase in percentage of NK1.1^{+} TCRβ^{-} cells in tumors of IL-27R deficient mice compared to IL-27R sufficient controls (Fig. 2E,F), which was unlikely due to changes in NK cell proliferation as no difference in BrDU incorporation was detected (data not shown). The NK1.1^{+} TCRβ^{-} population consists of at least two different cell lineages: *bona fide* NK cells and innate lymphoid cells type 1

(ILC1) (49,50). While these two lineages were proposed to develop via distinct pathways, they have a lot of phenotypic and functional similarities with some degree of organ- and disease-related specificity (51) complicating the unequivocal discrimination between these subsets (49,50,52). To better characterize NK1.1^{+}TCRβ^{-} population and further distinguish NK cells and ILC1, we first performed FACS staining for Eomes, Perforin, CD49a and CD49b markers. We found that the NK1.1^{+}TCRβ^{-} population in non-tumor and tumor liver tissue contains both NK cells (Eomes^{+}Perforin^{+}CD49b^{+}NK1.1^{+}TCRβ^{-}) and ILC1 (Eomes^{-}Perforin^{-}CD49a^{+}NK1.1^{+}TCRβ^{-}); and that *bona fide* NK cells outnumbered ILC1 (Fig. 2G, H, Supplementary Fig. S3D). While both populations had been detected, CD49b^{+} NK cells but not CD49a^{+} ILC1 cells were found to be significantly increased in tumors of DEN-treated *Il27ra*$^{-/-}$ mice (Fig. 2G,H).

Analysis of human HCC gene expression data using CIBERSORT for NK cell proportion estimations confirmed a significant, but relatively small negative correlation between the presence of NK cells and *IL27RA* and *IL27EBI3* expression in tumors (Fig. 2I). Moreover, analysis of published human HCC scRNAseq data (53) also showed a negative correlation between *IL27RA* expression and NK cell activation signature (Fig. 2J). These data altogether suggest that expression of cytokine IL-27 or its receptor negatively correlates with the presence of NK cytotoxic cells both in mouse and human HCC.

IL-27R acts as immunological checkpoint, taming innate cytotoxic lymphocyte activation in HCC

To further gain insights into the role of IL-27R signaling in the control of innate lymphoid and NK cell function and cytotoxicity in HCC, we performed flow cytometry analysis of NK1.1^{+} cells from non-tumor and tumor tissues and found that ablation of *Il27ra* led to the upregulation of Granzyme B (Fig. 3A). Q-RT-PCR analysis of FACS sorted NK1.1^{+}TCRβ^{-} cells from HCC tumors and adjacent normal tissues revealed the upregulation of *Gzmb* and *Tnfsf10* mRNA, implying enhanced activation and cytolytic potential of these cells (Fig. 3B). We also observed an upregulation of *Cxcr6* in NK1.1^{+}TCRβ^{-} cells from *Il27ra*$^{-/-}$ mice (Fig. 3B), a chemokine receptor that is characteristically expressed on hepatic innate cytotoxic cells and known to regulate their accumulation (54,55).

To further elucidate the role IL-27R signaling in NK and other cells in HCC, we performed scRNAseq of FACS-sorted Live/Dead^{-}CD45^{+} NK1.1^{+} and NK1.1^{-} cells from non-tumor and tumor tissues of DEN-treated *Il27ra*$^{-/-}$ and *Il27ra*$^{+/-}$ mice using droplet-based 10× Genomics Chromium scRNAseq (Supplementary Fig. S4A,B). The resulting quality controlled single cell atlas included 41,772 cells that were clustered based on Seurat's graph-based clustering approach (56) and visualized using a uniform manifold approximation and projection (UMAP) plot. Cluster annotation and identification was corroborated using overlapping marker genes from Immgen and previous transcriptional profiling of mouse NK and innate lymphoid cells (ILCs) (57) (Supplementary Fig. S4C). The combined analysis of all captured CD45^{+}NK1.1^{+} and CD45^{+}NK1.1^{-} cells revealed the presence of 34 clusters comprising at least 19 different immune cell types (Supplementary Fig. S4D). Similar to the data from human HCC (Fig 1 H–J), *Il27ra* expression was observed on many hematopoietic cells with the highest expression on NK and various

T cell subsets, while *Il27Ebi3* cytokine expression was restricted mostly to myeloid cell subsets (Supplementary Fig. S4E). As heightened accumulation of NK1.1^{+} cells was detected in tumors of *Il27ra*$^{-/-}$ mice, we further concentrated on scRNAseq analysis of Live/Dead^{-}CD45^{+} NK1.1^{+} cells. Clustering analysis revealed the presence of NK cells, ILC1 and NKT cells among 9511 sorted NK1.1^{+} cells (Fig. 3C), among which we identified 2 clusters of ILC1(1642 cells) and 7 clusters of NK cells (4376 cells) (Fig. 3D). Cell type-specific gene expression analysis further confirmed the specificity of the clusters (Supplementary Fig. S5A–E). PERMANOVA analysis of gene expression between *Il27ra*$^{-/-}$ and *Il27ra*$^{+/-}$ tumor samples for NK and ILC1 clusters showed the most significant changes in NK clusters 3 and 5, while less significant changes were found in ILC1 clusters 2 and 4 (Fig. 3E). Therefore, we decided to further elucidate transcriptional changes among NK and ILC1 cells and their dependence on IL-27R signaling. First, we performed trajectory analysis that identified 3 potential trajectories of NK cell differentiation that start from the least differentiated (or immature) cluster 7. Two of the trajectories progress towards clusters 1, 3 and 5 (Fig. 3F, Supplementary Fig. S6A). Importantly, initial recruitment of NK cells was elevated (cluster 7) in tumors of *Il27ra*$^{-/-}$ mice, while cell numbers at the intermediate stages (clusters 0,6,8) were depleted at the expense of increased numbers of NK cells progressing through the trajectories towards terminal clusters 1,3,5 in the absence of IL-27R signaling (Fig. 3G). KEGG pathway analysis of differential gene expression (DEG) along the trajectory demonstrates upregulation of several metabolic pathways and NK cell cytotoxicity genes along the differentiation trajectory towards more mature clusters (Fig. 3H). Indeed, changes in cellular metabolism have been previously linked to enhanced NK cell activation and cytotoxicity (58,59). In order to gain insights into the cluster identity along the trajectories, we first performed pseudotemporal ordering of single cell transcriptomes, which revealed that NK cell differentiation trajectories indeed move towards more mature cytotoxic effectors (clusters 1,3,5), as suggested by upregulation of cytotoxic genes *Gzmb* and *Prf1*, downregulation of “immature” genes *Emb*, *Kit* and *Il7r*, and no changes in *IFNγ* (Fig. 3I; Supplementary Fig. S6B). DEG analysis showed that intratumoral NK cells from *Il27ra*$^{-/-}$ mice were more activated (*Orai1, Nfatc1, Litaf, Irf8, Ifngr1, Ifnar, Tnfsf1a,Tnfsf1b, Il21r, Dgat1, Nfil3* were upregulated; whereas *Ccl3, Ccl4, Atf3, Dusp2, Zfp36, Car2* were downregulated) (60–63). They also expressed lower levels of inhibitory receptors (*Klrc1, Klrc2, Klre1*) known to interact with HLA-E, which regulates NK cell anti-tumor activity (63). The expression of various motility genes (*Tubb2a, Tubb4b*) (64) was enhanced and *S1pr5* was downregulated, suggesting activation and retention of NK cells in the tissue. Lastly, the expression of cytotoxicity genes (*Gzmb, Prf1* and *Serpinb9*) (65) was also enhanced (Fig. 3J). Overall, these data imply that ablation of IL-27R signaling enhances activation and cytotoxicity of NK cells and induces their differentiation towards more mature subsets. On the contrary, IL-27 signaling deters acquisition of maturity and cytotoxicity by NK cells, thereby playing an immunoregulatory role.

Among ILC1 cells, we identified two clusters (Fig. 3D) and established the trajectory of their differentiation from cluster 4 to cluster 2 (Fig. 3K, Supplementary Fig. S6C) as the absence of IL-27R increases the differentiation of “cytotoxic-like” ILC1 (cluster 2) at the expense of “conventional” ILC1 in cluster 4 (Fig. 3L). Pseudotemporal ordering of single cell transcriptomes revealed the upregulation of *Gzmb,* but not *Prf1,* while the expression

of markers of immature cells (*Il18r1, Tcf7* and *Kit)* was reduced during the progression from cluster 4 to cluster 2. No difference in *Ifng* was detected (Fig. 3M, Supplementary Fig. S6D). However, we found an upregulation of *Gzmb, Gzma, Gzmc, Serpin6b, Fasl, Il21r, Dgat1, Cd7, Ccr5, Cd160, Itga1* and *Nfil3* and downregulation of *Atf3, Dusp2, Zfp36, Hif1a* and *Id2* genes, similar to recently described (65) transcriptional changes during ILC1 differentiation towards "cytotoxic-like" ILC1 (Fig. 3N). KEGG pathway analysis further confirmed upregulation of TNF signaling and "NK cell cytotoxic pathways" in ILC1 (Fig. 3O). Therefore, IL-27R signaling represses the emergence of "cytotoxic" profile in a subset of ILC1 similar to its function in NK cells. Ridgeline plot visualization of gene expression across multiple clusters of tumor NK and ILC1 cells further demonstrated the upregulation of representative cytotoxicity genes *Gzmb*, *Faslg* and *Prf1* and chemokine receptor *Ccr5* in NK clusters 1,3,5 in tumors of *Il27ra*$^{-/-}$ mice compared to *Il27ra*$^{+/-}$ controls (Supplementary Fig. S5B). While the loss of IL-27R also induced cytotoxic gene expression in ILC1 (cluster 2), the level their expression in ILC1 cells was lower compared to NK cells, especially for a key cytotoxic marker *Prf1* (Supplementary Fig. S5B). The expression of anti-tumorigenic *Ifng*, which also functionally defines ILC1, was similar between NK and ILC1 populations and did not depend on IL-27R signaling (Fig. 3I, M; Supplementary Fig. S6B, D).

Altogether, scRNAseq analysis of tumor NK1.1^{+} revealed that in HCC, NK cells outnumber ILC1, IL-27R signaling negatively regulates terminal differentiation of intratumoral NK cells and ILC1 towards cytotoxic phenotype, and ablation of IL-27R signaling alleviates this differentiation block and promotes the expression of the cytotoxic program.

NK cell activation is controlled by multiple activating and inhibitory receptors, which regulate their "active" versus "inactive" state (66). NKG2D activating receptor engagement by "stress molecule" ligands on target cells increases NK cell activity (54,67–70), while inhibitory receptor Ly49C engages MHC class I (H-2K^{b} and H-2D^{b}) on target cells and dampens NK cell activation (67,71,72). We found an upregulation of activating receptor NKG2D (Fig. 4A,B) and downregulation of inhibitory receptor Ly49C (Fig. 4C) specifically on CD49b^{+} NK cells from HCC tumors of *Il27ra*$^{-/-}$ mice. These data are in agreement with scRNAseq results showing downregulation of multiple inhibitory receptors, including *Klrc1, Klrc2* and *Klre1* in NK cells from *Il27ra*$^{-/-}$ mice (Fig. 3J). No significant changes in NKG2D or Ly-49C expression were detected in blood or splenic NK1.1^{+}CD49b^{+} NK cells or liver NK1.1^{+}CD49a^{+} ILC1 suggesting organ- and cell type specificity (Supplementary Fig. 7A–C). Next, we used conventional flow cytometry markers of NK cell maturation and found an elevated presence of terminally differentiated mature cytotoxic CD11b^{+}CD27^{-} NK cells (73) in HCC tumors from *Il27ra*$^{-/-}$ mice, while less mature CD11b^{+}CD27^{+} NK cells were found in tumors of *Il27ra*$^{+/-}$ controls (Fig. 4D) similarly to observed in scRNAseq.

To further understand the functional implication of IL-27 signaling in regulation of NK cell activity, we performed *ex vivo* cytotoxicity and degranulation assays. Sorted NK cells were co-cultured with YAC1 target tumor cells followed by the analysis of killing efficiency and degranulation of CD49a^{+} ILC1 or CD49b^{+} NK cells (Fig. 4E–G). We found that cytotoxicity of both liver and spleen derived cells was elevated in the absence of IL-27R, while liver NK cells were more efficient killers (Fig. 4F). The ability of CD49b^{+} *Il27ra*$^{-/-}$ cells to degranulate was also heightened (Fig. 4G). Next, we performed *in vivo* cytotoxicity assay

with RMA-S (sensitive to NK killing) and RMA (insensitive) cell lines which were labelled with fluorescent dyes and injected i.p. at 1:1 ratio into naive *Il27ra*$^{-/-}$ or *Il27ra*$^{+/-}$ mice. FACS analysis of the peritoneal lavage 48h after cells administration revealed a substantial reduction of RMA-S NK sensitive cells in *Il27ra*$^{-/-}$ mice compared to *Il27ra*$^{+/-}$ controls, indicating more efficient NK cell mediated cytotoxicity (Fig. 4H,I). This further supported our *ex vivo* observations and demonstrated enhanced NK cell cytotoxicity in the absence of IL-27R signaling.

To test whether IL-27 can directly regulate NK cells, sorted NK and ILC1 cells from spleen and liver of wild type mice were stimulated *in vitro* with rIL-27. IL-27 suppressed the expression of various cytotoxic and activating genes including *Gzmb*, *Faslg*, *Ifng* and *Klrk1* (Fig. 4J) in CD49b^{+} NK liver cells. CD49a^{+} ILC1 cells demonstrate different responses to rIL-27 stimulation and did not downregulate cytotoxic genes *Gzmb* and *Klrk1* in contrast to CD49b^{+} cells (Supplementary Fig S7D). Splenic CD49b^{+} NK cells showed lower responsiveness to rIL-27 stimulation (Supplementary Fig. S7E), confirming site and organ specificity.

In order to further characterize the link between immediate liver injury, IL-27R signaling and NK cell accumulation, we analyzed livers from mice subjected to acute carcinogen-induced liver injury. Eight-week-old *Il27ra*$^{+/-}$ and *Il27ra*$^{-/-}$ mice were administered with 100 mg/kg DEN, and gene expression in the liver was analyzed 48 hours later by Q-RT-PCR. We found strongly elevated expression *of Cxcl9* and *Cxcl10* chemokines as well as *Prf1* and *Tnfsf10* in the livers of DEN-treated *Il27ra*$^{-/-}$ mice (Supplementary Fig. S7F,G), indicating that IL-27R controls innate cytotoxic cell recruitment and cytotoxicity both during early and late stages of HCC development and may counteract early immunosurveillance exerted at the level of tumor seeding.

Taken together, these data suggest that IL-27R signaling is implicated into the control of innate cytotoxic cell accumulation, activation and cytotoxicity in the liver during HCC development, affecting NK cells, which are most abundant, and also ILC1 cells.

IL-27R signaling regulates the expression of NK cell activating “stress” ligands

In addition to the acquisition of mature functional cytotoxic program, NK cells require engagement of activating receptors on NK cells with corresponding stress-induced ligands on target cells and a loss of inhibitory signals from MHC I complexes. In particular, NK cell activation is dependent on RAE-1 and H60 families of activating “stress” ligands (74,75) and is further enhanced by MHC I downregulation, a “missing self” signal on target cells (76). The analysis of “stress” ligand expression in normal or tumor tissues of mice with DEN-induced HCC revealed a significant upregulation of *Raet1* and *H60b* expression in tumors of *Il27ra*$^{-/-}$ mice (Fig. 4K), which was confirmed by flow cytometry and IHC (Fig. 4L,M). Conversely, rIL-27 was able to suppress *Raet1* and *H60b* expression in HCC cells (Fig. 4N). Furthermore, a significant downregulation of surface MHC I expression was observed on tumor cells in DEN-*Il27ra*$^{-/-}$ mice compared to *Il27ra*$^{+/-}$ controls (Fig. 4O), along with a reduction in *Tap1* expression, a regulator of MHC class I peptide loading (Fig. 4P). These data imply that IL-27R signaling promotes expression of MHC I and represses

upregulation of NK-triggering “stress” ligands on tumor cells, thereby serving as an indirect and direct immunoregulator of NK cell activity and NK cell mediated anti-tumor responses.

IL-27R signaling regulates NK cells and drives NASH-induced HCC

While the incidence of liver cancer caused by hepatitis B and C declines due to efficient vaccines and therapies (77), obesity-driven HCC is on the rise (9,78). Obesity drives the development of non-alcoholic steatohepatitis (NASH), strongly promoting HCC (79). To complement our studies performed in carcinogen-induced DEN model, we next sought to generalize our observations using a NASH-dependent model of HCC. We crossed *Il27ra*$^{-/-}$ and *MUP-uPA* mice where the *uPA* (urokinase plasminogen activator) transgene is controlled by the mature hepatocyte-specific promoter (*MUP*). *MUP-uPA* expression combined with Western diet (WD) feeding drives strong fibrosis, steatosis and spontaneous HCC development, producing overall faithful model of NASH-driven HCC similar to humans (80–82). *MUP-uPA*$^{+}$*Il27ra*$^{-/-}$ and *MUP-uPA*$^{+}$*Il27ra*$^{+/-}$ control mice were fed the WD starting at 8 weeks of age for a total period of 8 months. Similar to observations in the DEN-induced HCC model, IL-27R deficient *MUP-uPA*$^{+}$ mice were largely protected from cancer development (Fig. 5A, B), while no significant difference in body weight was found (Supplementary Fig. S8A). Tumors from *MUP-uPA*$^{+}$*Il27ra*$^{-/-}$ mice were characterized by the reduction of *Ccnd1* and *Lcn2* expression (Fig. 5C,D), implying reduced proliferative capacity of tumors and inflammation in the absence of IL-27R signaling. Augmented fibrosis is associated with fatty liver disease and is driving HCC development (83). We found a reduction of fibrosis in livers of *MUP-uPA*$^{+}$*Il27ra*$^{-/-}$ mice compared to controls as determined by Van Gieson and Trichrome (Fig. 5E,F) and anti-αSMA IHC stainings (Supplementary Fig. S8B). These data suggest that IL-27R signaling is implicated in the control of liver fibrosis and NASH-driven HCC.

Analysis of published scRNAseq data from livers of mice developing NASH (84) further confirmed the cell-specific pattern of IL-27R and IL-27 cytokine subunits expression (Supplementary Fig. S8C–F), similarly to observed in mouse and human HCC (see Fig. 1H–J and Supplementary Fig. S4D). No changes in CD4 or CD8 T cells (Fig. 5G), but elevated accumulation of NK1.1^{+}TCRβ^{-} cells in tumors of *MUP-uPA*$^{+}$*Il27ra*$^{-/-}$ mice (Fig. 5H) were detected by flow cytometry. Among NK1.1^{+}TCRβ^{-} cells, CD49b^{+}NK1.1^{+} (NK cells) were significantly upregulated in tumors of *Il27ra*$^{-/-}$ mice (Fig. 5I) along with heightened expression of *Cxcr6* and *Gzmb* (Fig. 5J). Consistent with the results in the DEN model, we detected elevated expression of *Raet1* and *H60b* in tumors of IL-27R deficient *MUP-uPA*$^{+}$ mice (Fig. 5K) while MHC I and *Tap1* were downregulated (Fig. 5 L,M). These data further advanced a functional and mechanistic link between IL-27R signaling and regulation of natural cytotoxic cell mediated anti-tumor immunity and tumorigenesis in an independent model of HCC of different etiology.

Tumor promoting effect of IL-27R signaling is exerted through suppression of innate cytotoxic cells-mediated anti-tumor immunity

Next, we sought to establish the “linear” mechanistic link between IL-27R signaling, NK cell activity and HCC. We first tested whether NK cells are essential for the anti-tumor effect of IL-27R ablation. We depleted NK (and ILC1) cells using anti-NK1.1 antibody in

DEN-treated *Il27ra*$^{-/-}$ and *Il27ra*$^{+/-}$ mice for a total period of 5.5 months prior to tumor development evaluation. Efficiency of NK depletion was confirmed by FACS analysis of blood, non-tumor and tumor tissues (Supplementary Fig. S9A,B). The depletion of NK1.1^{+} cells enhanced tumor growth in *Il27ra*$^{-/-}$ mice and eliminated the differences between *Il27ra*$^{-/-}$ and *Il27ra*$^{+/-}$ cohorts (Fig. 6A,B), suggesting that innate cytotoxic cells are one of the key functional immune populations regulated by IL-27R in the context of HCC tumorigenesis. The depletion of NK1.1^{+} cells also augmented liver fibrosis in both IL27R deficient and sufficient mice, eliminating the difference between genotypes (Fig. 6C and Supplementary Fig. S9C,D).

NKp46 is a natural cytotoxicity receptor expressed by NK cells essential for their activation (85). FACS analysis of liver NK cells confirmed elevated NKp46 expression in *Il27ra*$^{-/-}$ mice compared to *Il27ra*$^{+/-}$ controls (Fig. 6D). Moreover, *in vitro* stimulation of sorted CD49b^{+} NK cells with rIL-27 suppressed NKp46 (*Ncr1*) expression, suggesting that IL-27R signaling could be at least partially involved in the regulation of this cytotoxicity receptor and therefore may impact the functional activity of NK cells (Fig. 6E). We, therefore, took advantage of the NKp46-GFP reporter strain (*Ncr1*^{gfp}), where the *Ncr1* gene is replaced by green fluorescent protein (GFP) (86). Heterozygous or homozygous disruption of NKp46 in these mice was shown to affect expression levels of NKp46, impacting cell activation and differentiation (87). We crossed *Ncr1*^{gfp} to *Il27ra*$^{-/-}$ mice to assess HCC development. *Ncr1*$^{+/gfp}$*Il27ra*$^{-/-}$ and *Ncr1*$^{+/gfp}$*Il27ra*$^{+/-}$ mice were administered with DEN as described above, and tumor development was analyzed at 10 months of age. Similar to NK cell antibody depletion, reduced NK cell activation capacity in *Ncr1*$^{+/gfp}$ mice negated the anti-tumor effect of IL-27R deficiency and resulted in similar tumor load and number of tumors formed in IL-27R deficient and IL-27R sufficient mice (Fig. 6F,G; see Fig.1K, L for comparison). Importantly, heterozygous *Ncr1*$^{+/gfp}$ status did not affect tumor development in IL-27R sufficient mice. Therefore, we conclude that not only the presence, but also the activation of cytotoxic NK and possibly ILC1 cells is required for the anti-tumor effect of IL-27R deficiency.

Pharmacological inhibition of IL-27 signaling suppresses HCC.

In order to test the therapeutic potential of IL-27/IL-27R signaling inhibition, we used an IL-27 neutralizing antibody (SRF381), which binds to IL-27p28 and blocks IL-27-induced signaling (Supplementary Fig. S10A–C). *MUP-uPA*$^{+}$ mice were fed a WD for a period of 8 months and treated with SRF381 antibody or isotype control for the last 3.5 months. We found a significant reduction of HCC in mice that received SRF381 compared to IgG2a isotype controls (Fig. 7A–C). Administration of anti-IL-27 antibody also suppressed fibrosis as determined by Trichrome and anti-α-SMA staining (Fig. 7D,E). Flow cytometry analysis revealed no alterations in CD8 or CD4 T cells (Fig. 7F), but an increased presence of NK1.1^{+} cells in tumors of mice that received anti-IL-27 (Fig. 7G). Gene expression analysis showed upregulation of *Gzmb, Tnfsf10*, *Klrk1*, and *Cxcr6* in non-tumor and tumor tissue of mice that received SRF381 (Fig. 7H), suggesting that neutralization of IL-27 suppresses HCC via upregulation of innate cytotoxic mechanisms.

Furthermore, to assess the feasibility of therapeutic IL-27R receptor blockade and to establish that both IL-27 ligand and receptor are essential, we performed pharmacological inhibition of IL-27R. Anti-IL-27R or control antibody were administered to WD-fed *MUP-uPA*$^{+}$ mice for the last 4 months of WD feeding. Similar to genetic models and IL-27 neutralization, we found that pharmacological blockade of IL-27R also suppressed tumor growth (Fig. 7I–K), establishing an important role for the IL-27 pathway in HCC tumorigenesis.

Overall, our data suggest that IL-27R signaling controls HCC tumor development *in vivo* through a new immunological checkpoint regulating innate cytotoxic NK and ILC1 cells. Particularly, we found that IL-27R signaling suppressed NK cell accumulation, terminal differentiation and activation by controlling the expression of cytotoxic program, activating and inhibitory receptors on NK cells, as well as MHC I and stress-induced ligands on cancer cells. Pharmacological inhibition of IL-27 or its receptor significantly suppressed HCC development and growth, implying that the IL-27 pathway may serve as a promising therapeutic target for patients with this devastating disease.

Discussion

Primary liver cancer is the fifth most common cancer worldwide, accounting for over 800,000 deaths each year (88). Despite efforts to curb HCC via implementation of vaccines against hepatitis B and drugs against hepatitis C, the incidence of liver cancer is sharply on the rise, because of the increased prevalence of fatty liver disease coupled with the epidemic of obesity and type II diabetes as well as increased exposure to environmental toxins and pollutants (88). While chronic inflammation is known to contribute to liver cancer development, mechanisms of anti-cancer immune responses in HCC are not completely understood. Since many patients with chronic liver disease are set to progress to HCC at some timepoint, approaches to curb HCC progression and new avenues for HCC therapies are in dire need.

IL-27 and its receptor signaling have been implicated in the regulation of inflammation in various acute and chronic inflammatory diseases (23,36,38,40,89). The role of IL-27 in cancer development remains controversial and has not been extensively investigated in faithful *in vivo* models. While IL-27 was originally described as a pro-inflammatory cytokine, subsequent studies demonstrated its largely anti-inflammatory role, placing IL-27 into the clan of immunoregulatory cytokines (90). We and others have previously shown that inactivation of IL-27R in chronic inflammatory diseases results in enhanced inflammation and production of IL-6, IL-17A and other cytokines (23,24,39), suggesting that, perhaps in HCC, IL-27 would play an anti-inflammatory role limiting pro-tumorigenic inflammation, and that IL-27R signaling inactivation will result in heightened HCC development.

Here we found that elevated *IL27RA* mRNA expression correlates with more advanced stages of HCC and poor survival since the initial treatment in TCGA, LCI and SNU HCC patient cohorts. Moreover, we found that patients with HCC have elevated serum levels of the IL-27EBI3 subunit compared to healthy controls which is in line with a recent prospective cohort study where serum IL-27 was found to be predictive of de novo HCC

formation in patients with liver disease (91). Furthermore, using two different *in vivo* models of HCC, a carcinogen-induced injury-promoted (DEN) model and NASH-driven (MUP-uPA) model, we found that genetic inactivation of IL-27R suppressed HCC.

The liver microenvironment is uniquely enriched for NK cells, where they also exert immune surveillance (16). NK cells are potent killers of senescent, infected or cancerous cells and participate in regulation of immune responses via the production of inflammatory cytokines in the normal liver (16). During HCC development, the number and activation of liver NK cells are gradually reduced due to the chronic exposure to a yet unidentified, presumably tumor-derived stimulus and reduction in the expression of NK cell attracting chemokines (18). As obesity-induced NASH is one of the major drivers of HCC, it is important to note that NK cell number and function are also reduced in fatty liver disease (92). The emerging mechanism of IL-27R signaling promoting HCC relied on the inhibition of anti-cancer immune responses, particularly through controlling the accumulation and activation of NK1.1 innate cytotoxic cells, including NK and ILC1. While some surface markers, such as CD49b on NK cells, and CD49a and CD200R1 on ILC1, can distinguish between these two subsets of cells, the majority of cell surface markers are similar and in most cases only subtle changes in their expression allows for discrimination between these two populations (49). While both cell populations are capable of performing cytotoxic and cytokine-producing functions, NK cells are believed to be more cytotoxic, while ILC1 are more potent producers of cytokines, including IFNγ. Recent work, however, demonstrated the ability of ILC1 to differentiate towards more cytotoxic subpopulation (49,65). Furthermore, NK and ILC1 cells are characterized by evident organ- and disease specific phenotypes and responses, which further complicate the unequivocal, simultaneous analysis of their comparative physiological roles (52). Single cell RNA sequencing of $NK1.1^{+}TCR\beta^{-}$ cells revealed enhanced NK and ILC1 cell differentiation toward more mature, more cytotoxic subpopulations in the absence of IL-27R, implying that in the context of liver cancer, IL-27R signaling plays an important suppressive role in the regulation of innate cytotoxicity. While the presence of both ILC1 and NK cells have been detected in our models of liver cancer, and IL-27R signaling repressed cytotoxicity in both populations, $CD49b^{+}$ NK cells outnumbered ILC1 and were elevated in the absence of IL-27R signaling. Importantly, in HCC tumors levels of the key anti-tumorigenic cytokine IFNγ were unchanged by IL-27R status in NK cells or ILC1, arguing that a cytokine producing function of NK and ILC1 cells is unlikely to be the key mediator of IL-27R signaling in HCC. An upregulation of IL-15, a cytokine driving NK cell maturation and differentiation, in *Il27ra*$^{-/-}$ mice could explain enhanced NK cell maturation and cytotoxicity observed in naive and tumor-bearing mice, but IL-27R-dependent mechanisms regulating IL-15 requires further investigation.

The depletion of $NK1.1^{+}$ cells during HCC development demonstrated that the effect of IL-27R signaling on HCC is indeed largely dependent on these cells despite specificity limitations of this approach (47), which affects NK, ILC1 and NKT cells. The role of NKT cells in HCC is not fully understood. NKT cells have been shown to play both anti- and pro-tumorigenic role in HCC particularly depending on NASH-related or carcinogen-related etiology (93–95). Importantly, IL-27R signaling ablation or neutralization uniformly reduced HCC in DEN-induced and NASH-induced models in agreement with poor prognosis

regardless of viral or obesity status in patients with HCC. In addition, while being more restricted to NK and ILC1 cells, partial functional impairment of cell activation in *Ncr1*$^{+/gfp}$ mice still resulted in enhancement of cancer development in *Il27ra*$^{-/-}$ mice similar to observations with NK1.1^{+} cell depletion. These data support the importance of IL-27R signaling in the control of natural cytotoxic cells but additional work will be needed to address possible involvement of NKT cells.

The execution of NK cell cytotoxicity against target cells requires the engagement of activating receptors, and is further regulated by the balance between activating and inhibitory receptor signaling (66). We observed that CD49b^{+} NK cells isolated from HCC tumors in the absence of IL-27R signaling exhibit upregulation of activating receptor NKG2D and downregulation of inhibitory receptor Ly49C (Fig. 4A). Single cell RNA seq data also confirmed a downregulation of multiple inhibitory receptors (Fig. 3J). While IL-27R signaling has been previously shown to regulate NK cell function (96,97), the outcomes were largely context dependent, the disease model used and tissue localization of NK cells, and not specifically attributed to NK cells or ILC1. For example, IL-27 together with IL-12 and IL-2 has been shown to promote NK cell activity *in vitro* (96). However, our data demonstrate that *in vitro* stimulation of sorted liver CD49b^{+} NK cells with rIL-27 downregulated gene expression of cytotoxic molecules such as granule components (*Gzmb, Prf1*), FasL (*Faslg*) and NKG2D (*Klrk1*), but it had limited effect on splenic CD49b^{+} NK cells. Overall, these *ex vivo* and *in vitro* experiments supported our observations of heightened cytotoxicity of NK cells in *Il27ra*$^{-/-}$ HCC tumors, suggesting a direct suppressive function of IL-27R on NK cells that regulates cytotoxic programs and balances activating and inhibitory receptor signaling.

Expression of so-called “stress ligands” on the surface of cancerous cells as well as the reduction of MHC I expression to avoid T cell immunity represent a “second signal” required to enable NK cell cytotoxicity (74,76). Our data revealed elevated expression of NK cell-stimulating stress ligands (*Raet1*, *H60b*) and reduction in *Tap1* MHC I-processing molecule and surface MHC I expression in HCC tumors of *Il27ra*$^{-/-}$ mice. Moreover, the direct stimulation of HCC cells with rIL-27 suppressed *Raet1* and *H60b* expression, suggesting a potential mechanism of how IL-27R may indirectly regulate NK cell activation and cytotoxicity. Of note, no direct effect of IL-27R signaling on the proliferation of normal or transformed hepatocytes had been observed in the cell autonomous system where immune cells are not present, indicating that regulation of stress ligands phenotypically displays itself only within complete tumor microenvironment harboring innate cytotoxic lymphocytes. Our data together with recently published work on the overexpression IL-27R in hepatocytes (98) paves the road to further examine additional roles of hepatocyte-specific IL-27R signaling in HCC, as well as possible involvement of IL-27R signaling in other immune and non-immune cell types.

Apart from the direct regulation of NK cells, IL-27 can also regulate other cell types, which in turn could mediate NK cell accumulation and activation via cell contact interactions (PD-1, MHC I, 2B4-CD48) or via production of chemokines and cytokines affecting NK cell recruitment (CXCL9, CXCL10), their differentiation and/or maturation (IL-15, IL-12, IL-18, IL-10) (99). Towards this end, we found that acute DEN administration triggered

heightened expression of *Cxcl9* and *Cxcl10* chemokines and increased expression of NK cell effector molecules such as *Prf1* and *Tnfsf10* in the livers of IL-27R deficient mice 48 hours after DEN treatment. These observations are consistent with the scenario that IL-27R signaling represses the NK cell-based cancer immunosurveillance, thereby enhancing HCC tumor initiation.

With the global epidemic of obesity and type II diabetes, NASH-driven HCC is set to surpass all other forms of HCC in incidence (8,9). The *MUP-uPA* /WD HCC model faithfully resembles human HCC driven by fatty liver disease and fibrosis. We found that inactivation of IL-27R not only suppresses tumor development in this model, but also strongly reduces the underlying fibrosis. Similarly to DEN model, $MUP\text{-}uPA^{+}Il27ra^{-/-}$ mice also showed enhanced innate cytotoxic cell activation, implying existence of a common mechanism regulated by IL-27R signaling. Stellate cells and fibroblasts constituting fibrotic masses in NASH and HCC are often senescent (100), and NK cells were shown to kill senescent fibroblasts, thereby regulating fibrosis in liver disease (101,102). Enhanced NK cell cytotoxicity was indeed linked to limited fibrosis observed in $MUP\text{-}uPA^{+}Il27ra^{-/-}$ mice. Likewise, NK cell depletion resulted in enhanced fibrosis, especially evident in DEN-$Il27ra^{-/-}$ mice.

While several models of liver cancer are available, each of them has their advantages and limitations (80). Several earlier publications attempted to address the role of IL-27 in cancer development, particularly utilizing cell transplantation approaches, overexpression of IL-27 and IL-27R or rapid induction of multiple oncogenes in hepatocytes (32–34,98). While such models have clear advantages in terms of the fast and uniform tumor growth, they may be less perfect for studying mechanisms which rely on a competent tumor microenvironment and chronic inflammation, a key component regulated by cytokines in cancer. Our work here demonstrates that ablation or pharmacological neutralization of IL-27R signaling limits liver cancer development in two different faithful models of HCC: carcinogen- and injury-promoted HCC (DEN) and NASH-driven HCC (*MUP-uPA* +WD). Along with human data on poor survival, advanced tumor stages, and lower NK cytotoxicity signatures in $IL27RA^{high}$ HCC patients, and heightened serum level of IL-27EBI3 in patients with HCC, our work implies that IL-27 pathway may play a tumor-promoting role in HCC that is generalizable across different models and types of HCC with different drivers. An essential component of this mechanism is mediated through IL-27 dependent suppression of intratumoral innate cytotoxic cells, including NK cells and ILC1.

Taken together, our data uncover the important role of IL-27R mediated regulation of innate cytotoxic cells in mouse and human HCC, where it controls NK cell accumulation and activation as well as cytotoxicity of both NK and ILC1 cells. This process is amenable with neutralization of IL-27 or IL-27R to suppress HCC, suggesting that inhibition of IL-27 signaling represents potential therapeutic strategy in HCC and liver diseases with a high risk of progression to HCC.

Methods

Human Cohorts and data

In **CHUM cohort** serum was derived from whole blood obtained prior to HCC resection in 130 patients. Clinical data were collected prospectively by the CHUM Hepatopancreatobiliary Biobank, accredited by the Canadian tumor repository network (CTRnet). None of the patients had received chemotherapy or radiotherapy before surgery. In addition, serum was collected from 11 healthy donors without any medical history of cancer or hepatobiliary disease. Ethics approval for the study was obtained by the local institutional Ethics Board. Written informed consent was acquired from all of the patients.

Serum/plasma levels of EBI3 were determined with a custom sandwich Meso Scale Discovery (MSD) assay using EBI3 specific antibodies (SRF19557 as capture and SRF9D2 as detection). Briefly, MSD QUICKPLEX plates were prepared by coating each well with 40 µL of SRF19557 antibody diluted in PBS (0.5 ug/mL) and incubated overnight at 4C. Plates were then washed and blocked (1% FBS, 0.01% Tween 20 in PBS) for 1hr at room temperature (RT), followed by an additional wash. Individual samples from healthy controls or patients with HCC were diluted 1:2 in 0.1% FBS, 0.01% Tween 20 in PBS and 25 µL of sample was dispensed per well. The following control samples were tested on each plate: 1) Pooled serum (diluted 1:2) from pregnant women (2nd and 3rd trimester) known to contain high levels of EBI3(103); 2) Recombinant human IL-27 (R&D Systems or Peprotech) tested at several concentrations; 3) Serum from healthy donors diluted 1:2; and 3) diluent only. These samples were used as positive and negative controls to normalize values across plates. Samples were incubated for 2h at RT followed by washing and a subsequent incubation with the detection antibody SRF9D2 (0.5 µg/mL) for 1h at RT. Following another wash, a goat anti-murine SULFO-TAG labeled secondary antibody (diluted 1:1000, MSD) was added and incubated for 30 minutes at RT. Finally, plates were washed and MSD read buffer was added to each well before reading on the MESO QUICKPLEX SQ120 instrument. Raw MSD values were used to calculate EBI3 levels extrapolated from a standard curve of recombinant IL-27 (R&D systems). These EBI3 levels were then normalized across plates based on the values obtained from the pooled serum from pregnant women and a single concentration of rIL-27 (10 µg/mL Peprotech) and represented as “normalized EBI3”.

TCGA cohort

TCGA gene expression data were analyzed using Cox regression analysis for association of overall IL27RA expression with survival that does not require splitting patients into groups, but rather tests the association based on overall expression variation vs survival. Additionally top 25% expression cutoff was used to define correlation between *IL27RA* expression and disease-free survival. Continuous expression of *IL27RA* was also used in multivariate Cox regression analysis with age, gender and cancer grade as covariates. *IL27RA* was shown to be independent factor associated with survival showing p=0.0179 in this combined model. CIBERSORT NK cell proportion estimations were used to determine correlation between *IL27RA* expression and presence of NK cells in the tumors.

SNU and LCI cohorts.

We identified 233 paired HCC tumor and non-tumor samples from the LCI cohort (GSE14520)(42) and 70 HCC tumor samples from the SNU cohort (41). For LCI cohort, *IL27RA* expression of tumor tissue was compared to its paired non-tumor tissue, and tumors with the top 25% of *IL27RA* tumor-to-non-tumor ratio were defined as “high” *IL27RA* tumors, while the rest were defined as “norm”. For SNU cohort, where the information of non-tumor tissues was not available, ROC curve analysis with Youden index was used to identify the best cutoff value of *IL27RA* associates with overall survival, which was used to define “high”- and “norm” groups of tumors based on *IL27RA* mRNA expression.

Mice

Il27ra$^{-/-}$ (JAX#018078) and C57BL6/J (WT) (JAX#000664) mice were purchased from Jackson laboratory and crossed to obtain *Il27ra*$^{+/-}$ and *Il27ra*$^{-/-}$ mice. *Ncr1*$^{gfp/gfp}$ were obtained from Dr. Wayne Yokoyama (Washington University, St. Louis) and used to generate *Il27ra*$^{+/-}$ *Ncr1*$^{+/gfp}$, and *Il27ra*$^{-/-}$*Ncr1*$^{+/gfp}$. For NASH model *Il27ra*$^{-/-}$ mice were crossed to *MUP-uPA*$^{+}$ (104) to obtain *MUP-uPA*$^{+}$*Il27ra*$^{+/-}$ and *MUP-uPA*$^{+}$*Il27ra*$^{-/-}$ mice. All mice were on C57BL/6 background. The genotyping was performed by standard PCR protocols. Mice were housed and bred under specific pathogen-free conditions in an AAALAC-approved barrier facility at Fox Chase Cancer Center (FCCC) or Cedars-Sinai Medical Center (CSMC). Littermate and cagemate controls were used for all experiments. All animal experiments were approved by the Institutional Animal Care and Use Committee (IACUC) at FCCC and CSMC and performed in compliance with all relevant ethical regulations for animal research. Studies characterizing the activity of SRF381 were conducted according to guidelines established and approved by the IACUC at Mispro Biotech.

DEN model.—To induce HCC development 25 mg/kg of diethylnitrosamine (DEN) (Sigma-Aldrich, N0258) was administered i.p. into 15 day old male mice as described (45). Mice were maintained on autoclaved water and regular chow diet. HCC development was analyzed at 10 months of age. For acute response tissue were collected 48h after DEN (100mg/kg) administration.

NASH/HCC model.—*MUP-uPA*$^{+}$ *Il27ra*$^{+/-}$ and *MUP-uPA*$^{+}$*Il27ra*$^{-/-}$ female and male mice were fed the Western diet (Teklad, TD.88137) for 8 months beginning at 8 weeks after birth. HCC development was analyzed at 10 months of age.

Tumor number was calculated as the sum of all macroscopic tumors in liver. Tumor load was calculated as a sum of diameters of all the tumors per animal. Serum ALT was measured by ALT Activity Assay Kit (ab105134).

Antibody treatment—200 μg/mouse of anti-NK1.1 (produced from PK136 hybridoma, FCCC cell culture facility) or IgG2a (isotype control, FCCC cell culture facility) were injected i.p. weekly for 5.5 months starting from 4.5 months of age.

500 μg/mouse of anti-IL-27 (SRF381, Surface Oncology) or IgG2a isotype control antibodies were injected i.p. for last 3.5 months prior to tissue collection at 10 months. The human monoclonal antibody SRF381 was selected for binding to recombinant human IL-27, cross-reactivity to recombinant murine IL-27, and for blocking murine IL-27 mediated phosphorylation of STAT1 in splenocytes (see Supplementary Fig. S10). The Fc region of SRF381 was replaced with murine IgG2a.150 μg/mouse of anti-IL-27R (Amgen) or isotype control antibodies were injected i.p. for last 4 months prior to tissue collection at 10 months.

Cell lines

Cell lines were obtained from ATCC (YAC-1 (RRID: CVCL_2244), RMA (RRID: CVCL_J385), RMA-S (RRID: CVCL_2180). HCC cell lines were generated in cell culture facility of the Fox Chase Cancer Center from tumors of DEN injected *Il27ra*$^{-/-}$, *Il27ra*$^{+/-}$ and *Il27ra*$^{+/+}$ mice. All cell lines were used fewer than 10 passages before experiments were conducted. Cell lines were tested negative for *Mycoplasma* (2015) and have not been authenticated since first acquisition.

Histology and Immunohistochemistry

For histological analysis, a liver lobe (with tumors) was isolated and fixed in 10% buffered formalin (Fisher HealthCare, 23–245685) for 24 h. Five μm thick sections were prepared and stained with hematoxylin (Sigma-Aldrich, HHS32) and eosin Y (Thermo Scientific, 6766007). All images were acquired with Nikon Eclipse 80i microscope and EVOS Auto FL2.

A blinded pathology review of H&E slides from a subset of DEN-induced tumors and *MUP-uPA*-induced tumors did not reveal any meaningful differences between IL-27R deficient and control mice. Tumors in *Il27ra*$^{-/-}$ and control (*Il27ra*$^{+/-}$) mice showed a conventional moderately-differentiated HCC morphology with predominantly trabecular architecture. Tumor cells exhibited monomorphic nuclei and contained abundant cytoplasm with variable amounts of intracytoplasmic globules (a finding that can be seen in human HCC) and minimal to mild steatosis. The immune cell infiltrate was sparse in both *Il27ra*$^{-/-}$ mice and control mice. Occasional tumors exhibited prominent extramedullary hematopoiesis, but this was observed in both *Il27ra*$^{-/-}$ mice and control mice. Tumors in *MUP-uPA*$^{+}$*Il27ra*$^{-/-}$ and *MUP-uPA*$^{+}$*Il27ra*$^{+/-}$ mice showed the classic features of the steatohepatitic variant of HCC that arises in NASH in humans, as expected from previous reports describing the histopathological features of this model (80,81). Tumors in both *MUP-uPA*$^{+}$*Il27ra*$^{-/-}$ and control mice showed extensive steatosis (mixed small- and large-droplet, but predominantly large-droplet) and hepatocyte ballooning (swelling of tumoral cells with cytoplasmic degeneration and clumping of cytoplasmic contents). The nontumoral liver in both *Il27ra*$^{-/-}$ and control mice showed typical features of human NASH, with abundant steatosis and hepatocyte ballooning, more prominent in the centrilobular region (zone 3). The immune cell infiltrate was sparse in both genotypes. Given the similarity in histopathologic features between the two groups, tumor sequencing was not pursued.

For immunohistochemistry staining 5μm thick sections of livers containing tumors were deparaffinized by taking them through 4 changes in xylene, then washed by 4 changes in

100% ethanol followed by re-hydration in tap water. Antigen retrieval was performed in 1X Citrate buffer (Electron Microscopy Sciences, 64142–08) at 95°C for 1 h followed by 1 h cooling down to RT. Then slides were rinsed in tap water for 3 min and dehydrated in 100% ethanol for 1 min, followed by blocking in 3% H_2O_2 in PBS for 10 min. Slides were blocked with 5% goat serum in 1% BSA-PBS for 20 min, then they were incubated with primary antibody for Ki67 (1:100; BioLegend, 151202, RRID:AB_2566621), p-ERK1/2 (1:400; Cell Signaling, 4370, RRID: AB_2315112), IL-27R (34N4G11; Novus Biologicals, NBP2–19015, RRID:AB_2916313), α-SMA (1:500; Abcam, 124964, RRID:AB_11129103), RAE-1 (R&D, AF1136, RRID:AB_2238016), O/N at 4°C. After washing with 1% BSA-PBS slides were incubated with secondary goat anti-rat and goat anti-rabbit biotinylated antibodies for 30 min at RT followed by 30 min of incubation with streptavidin–HRP (1:500; BD Pharmingen, 554066). For developing DAB substrate (Invitrogen) was applied for 3 min followed by washing in water and counterstaining with Hematoxylin solution (Sigma-Aldrich, HHS32). Excess of Hematoxylin was removed by immersing slides in 0.25% ammonia water followed by rinsing in water. Slides were mounted with coverslips using Permount mounting medium solution (Fisher Chemical, SP15). All images were acquired with a Nikon Eclipse 80i microscope or EVOS Auto FL2. Microsoft PowerPoint was used for one step brightness adjustment for all images in parallel. Quantification was done using ImageJ (version 1.51).

Van Gieson staining

For collagen staining deparaffinized and re-hydrated slides were stained for 5 min in Van Gieson solution (EMS, 26374–06) followed by dehydration by 2 changes in 100% ethanol and cleared by 2 changes of xylenes. All images were acquired with Nikon Eclipse 80i microscope. Microsoft PowerPoint was used for one step brightness adjustment for all images in parallel. Quantification was done using ImageJ (version 1.51).

Masson's trichrome staining

For visualization of collagen fibers and histological assessment of collagen deposition, deparaffinized and re-hydrated slides were re-fixed in Bouin's solution for 1 h at 56°C, then rinsed in tap water for 5 min followed by staining with Weigert's iron hematoxylin working solution for 10 min. Slides were rinsed in tap water for 10 min and stained in Biebrich scarlet-acid fuchsin solution for 10 min followed by washing in distilled water, differentiated in the phosphomolybdic-phosphotungstic acid solution for 10 min or until the collagen is not red, and transferred to aniline blue solution for 5 min, rinsed briefly in distilled water and differentiated in 1% acetic acid solution for 2 min followed by wash in distilled water, dehydration and clearing in xylene. All images were acquired with an EVOS Auto FL2 microscope. Microsoft PowerPoint was used for one-step brightness adjustment for all images in parallel. Quantification was done using ImageJ (version 1.51).

Flow cytometry

Mice were sacrificed by CO_2 inhalation, and livers were perfused with HBSS containing 2% of Heparin (20 USP units/mL) to remove traces of blood. Livers were isolated, non-tumor and tumor tissues were dissected separately and incubated with a cocktail of digestion enzymes containing collagenase I (450 U/mL) (Sigma-Aldrich, C0130)

and DNase I (120 U/mL) (Sigma-Aldrich, D4263) in HBSS (with Ca^{2+}/Mg^{2+}) for 40 min at 37°C with gentle shaking at 150 rpm. After incubation, cell suspension was filtered through a 70 μm cell strainer. Immune cells were enriched by density-gradient centrifugation over Percoll (GE Healthcare, 17–0891–01) at 1000 g for 25 min without brake (40% Percoll in RPMI-1640 and 80% Percoll in PBS). Leukocyte ring on a border of gradient and parenchymal cells on top were collected, washed and stained. Spleens were isolated, mashed, and filtered through 70 μm cell strainers. Peripheral blood was collected by cardiac puncture and erythrocytes were lysed by red blood cell (RBC) lysis buffer (15 mM NH_4Cl, 0.1 mM $NaHCO_3$, 0.1 mM Sodium- EDTA) for 5 min at RT. The following antibodies were used to stain cells from liver, spleen or blood: CD45-PerCP (30F-11; BioLegend, 103130, RRID:AB_893339), CD11b-Pacific Blue (M1/70; BioLegend, 101224, RRID:AB_755986), NK1.1-FITC (PK136; BioLegend, 108706, RRID:AB_313393), NK1.1-PE (PK136; BioLegend, 108708, RRID:AB_313395), TCRβ-Alexa Fluor 700 (H57–597; BioLegend, 109224, RRID:AB_1027648), CD4-APC/Cy7 (GK1.5; BioLegend, 100414, RRID:AB_312699), CD8a-APC (53–6.7; BioLegend, 100712, RRID:AB_312751), Ly6G-APC/Cy7 (1A8; BioLegend, 127624, RRID:AB_10640819), Ly6C-PE/Cy7 (HK1.4; BioLegend, 128018, RRID:AB_1732093), F4/80-APC (BM8; BioLegend, 123116, RRID:AB_893481), Granzyme B-Pacific Blue (GB11; BioLegend, 515408, RRID:AB_2562196), CD27-PE/Cy7 (LG.3A10; BioLegend, 124216, RRID:AB_10639726), Ly49C-AF647 (4L03311), Ly-49I-PE (YLI-90; eBioscience, 1943023, RRID:AB_466020), NKG2AB6-APC (16A11; BioLegend, 142808, RRID:AB_11124538), NKG2D-PE (CX5; BioLegend, 130208, RRID:AB_1227712), CD49a-PE/Cy7 (HMa1; BioLegend, 142608, RRID:AB_2749931), CD49b-APC/Cy7 (DX5; BioLegend,108920, RRID:AB_2561458), CD11b-biotin (M1/70; BioLegend, 101204, RRID:AB_312787), CD31-PE (390; BioLegend, 102408, RRID:AB_312903), TER-119-biotin (TER-119; BioLegend, 116204, RRID:AB_313705), H-2Kb-PE/Cy7 (AF6–88.5; BioLegend, 116519, RRID:AB_2721683), H-2Kb/H-2Db-APC/Fire 750 (28–8–6; BioLegend, 114617, RRID:AB_2750197), Streptavidin-APC/Cy7 (BioLegend, 405208). All antibodies were used at 1:50 dilution and LIVE/DEAD Fixable Yellow Dead Cell stain (Invitrogen, L34959) at 1:200.

Gene expression analysis

Non-tumor and tumor tissues were homogenized in TRIzol reagent (Invitrogen, 15596018) with 2.8 mm ceramic beads (OMNI International, 19–646-3) using Bead Ruptor (OMNI International). Total RNA was extracted using Aurum Total RNA Fatty and Fibrous Tissue Kit (Bio-Rad, 7326870) according to the manufacturer's protocol. Sorted or treated cells were lysed in RLT Plus buffer (QIAGEN, 157030074) and total RNA was isolated using Rneasy Plus Mini Kit (QIAGEN, 74136) according to the manufacturer's protocol. Complementary DNA was synthesized using iScript Reverse Transcription Supermix (Bio-Rad, 1708841) with random primers according to the manufacturer's protocol. Q-RT-PCR was performed with Bio-Rad CFX 96 Connect Real-Time PCR Detection System using iTaq Universal SYBR Green Supermix (Bio-Rad, 1725124). The following primers were used: *Rpl32* (FW 5'-TTCCTGGTCCACAATGTCAA-3';REV 5'-GGCTTTTCGGTTCTTAGAGGA-3'), *Lcn2* (FW 5'-ATTTCCCAGAGTGAACTGGC-3';REV 5'-AATGTCACCTCCATCCTGGT-3'),

Ccnd1 (FW 5’-CTGGCCATGAACTACCTGGA-3’;REV 5’-GTCACACTTGATCACTCTGG-3’), *Cxcr6* (FW 5’-GAGTCAGCTCTGTACGATGGG-3’;REV 5’-TCCTTGAACTTTAGGAAGCGTTT-3’), *Gzmb (*FW 5’-CCACTCTCGACCCTACATGG-3’;REV 5’-GGCCCCCAAAGTGACATTTATT-3’), *Prf1* (FW 5’-CTGCCACTCGGTCAGAATG-3’;REV 5’-CGGAGGGTAGTCACATCCAT-3’), *Tnfsf10* (FW 5’-TCTGGTCCAGGGGTGTAAAG-3’;REV 5’-TGCTGACCTGCATTCATAGC-3’), *Faslg* (FW 5’-ACTCCGTGAGTTCACCAACC-3’;REV 5’-TTAAATGGGCCACACTCCTC-3’), *Ifng* (FW 5’-TGAACGCTACACACTGCATCTTG-3’; REV 5’-GACTCCTTTTCCGCTTCCTGA-3’), *Klrk1* (FW 5’-TCAAGCCAGCAAAGTGGGAT-5’;REV 5’-GGACTCGAACAACGAACATTGG-3’), *Raet1* (FW 5’-AGCACTTCACGTCACACCAG-3’;REV 5’-TATGGATACACCAACGGGCT-3’), *H60b* (FW 5’-AGCCTGAGAGAGCTTTCAGAA-3’;REV 5’-GGGTGTCAGAATTATGTTGGGAG-3’), *Tap1* (FW 5’-GGACTTGCCTTGTTCCGAGAG-3’;REV 5’-GCTGCCACATAACTGATAGCGA-3’), *Cxcl9* (FW 5’-TAGGCAGGTTTGATCTCCGT-3’; REV 5’-CGATCCACTACAAATCCCTCA-3’), *Cxcl10* (FW 5’-CCTATGGCCCTCATTCTCAC-3’;REV 5’-CTCATCCTGCTGGGTCTGAG-3’), *Il15* (FW5’-AATCAGATACCGCAATGACCAC-3’; REV 5’-CAGAAGTTGTTTGGGATGGTGT-3’).

NanoString

50 ng of tumor RNA was used for NanoString (Cancer Immunopanel) in order to analyze immune profile of the tumor microenvironment measuring the expression of 770 genes according to manufacturer’s protocol. The hybridization between target mRNA and reporter-capture probe pairs was performed at 65°C for 20 h using Applied Biosystems Veriti Thermal Cycler. All processing was carried out on a fully automated nCounter Prep Station. Excess of probes was removed and probe-target complexes were aligned and immobilized in the nCounter cartridge followed by the image acquisition and data processing by nCounter Digital Analyzer. The expression level of a gene was measured by counting the number of times the specific barcode for that gene was detected, and the barcode counts were then tabulated in a comma-separated value (CSV) format. The raw digital count of expression was exported from nSolver v3.0 software. Statistically significant differentially expressed genes between genotypes were analyzed by KEGG pathway analysis.

For cell prediction analysis, the data was normalized in R and batch corrected using ComBat-seq in the R package sva(105). The resultant datasets were analyzed using Gene Set Enrichment Analysis (GSEA) and compared to a gmx file containing gene signatures of all cell types that we derived in house from the Immgen database (www.immgen.org) and NK and ILC gene signatures from Robinette et al (57). The GSEA analysis was done in the GSEA software (106,107). Normalized enrichment scores were visualized using the ggplot2 package in R to represent abundance of different cell types in the data.

Clonogenic assay and HCC cell stimulation *in vitro*

1000 DEN-derived HCC cells were plated on a 0.1%-swine gelatin precoated 6-well plate in ACL-4 containing 20% FBS in triplicate per condition. 24 h later the medium was changed to ACL-4 containing 5% FBS with or without rIL-27 (200 ng/ml). On day 4 medium was refreshed and cells were left to grow for an additional 3 days. On day 7 after the beginning of the treatment the medium was aspirated, cells were washed with HBSS ($Ca2^+$/$Mg2^+$ free) and fixed 10% acetic and 10% methanol fixing solution for 15 min at RT. When the fixing solution was aspirated, plates were left to dry followed by adding 0.4% crystal violet staining solution for 20 min at RT. Rinsed with tap water wells were scanned with EPSON Perfection V600 Photo scanner.

For gene expression analysis 500,000 DEN-derived HCC cells were plated on a 0.1%-swine gelatin precoated 6-well plate in ACL-4 containing 20% FBS in triplicate per condition. 24 h later medium was changed to complete DMEM with 5%FBS with or without rIL-27 (200 ng/ml) for 3 h at 37°C in a 5% CO_2 cell culture incubator.

Partial hepatectomy

2/3 partial hepatectomy was performed as previously described (108). Briefly, mice were anesthetized by isoflurane. Skin and abdominal wall were cut open; left and right lobe were ligated sequentially with silk suture and excised. Then the abdominal wall was sutured and skin was clipped. Liver regeneration was analyzed in 8 days.

Western Blot

For Western blot analysis 500,000 DEN-derived HCC cells were plated on a 0.1%-swine gelatin precoated 6-well plate in ACL-4 containing 20% FBS in triplicate per condition. 24 h later medium was changed to complete DMEM without FBS with or without rIL-27 (200 ng/ml) for 0, 15 min, 30 min at 37C in a 5% CO_2 cell culture incubator.

Treated HCC cells were washed with HBSS ($Ca2^+$/$Mg2^+$ free) and lysed in RIPA buffer supplemented with phosphatase and protease inhibitors (Sigma-Aldrich, PPC1010) (200 μL per 106 cells) followed by centrifugation at 15,000×g for 10 min at 4°C to pellet not lysed cell debris. The supernatant was collected for analysis. Protein concentration was determined by BCA Protein Assay Kit (Sigma-Aldrich, 1001491004) according to the manufacturer's protocol. 40 μg of cell lysates were separated by 4–20% Tris-glycine MINI-PROTEAN TGX gels (Bio-Rad, 456–1094) and transferred to PVD membranes using Trans-Blot Turbo Transfer Pack (Bio-Rad, 1704156). Each membrane was washed with TBST (10 mM Tris-HCl, 150 mM NaCl, 0.1% Tween-20; pH 7.6) and blocked with 5% skimmed milk in TBST for 1 h followed by O/N incubation at 4 °C with appropriate primary antibody: phospho-STAT3 (D3A7; Cell Signaling Technology, 9145S, RRID:AB_2491009) and STAT3 (124H6; Cell Signaling Technology, 9139S, RRID:AB_331757). Loading was evaluated by staining with anti-β-actin-horseradish peroxidase (HRP) direct conjugate antibody (AC-15; Abcam, ab49900, RRID:AB_867494) (1:50000) for 1 h at RT. Each membrane was washed and primary antibodies were detected with a 1:5000 dilution of HRP-conjugated rabbit anti-mouse IgG (Cell Signaling Technology, 7076S, RRID:AB_330924) or mouse anti-rabbit IgG (Cell

Signaling Technology, 7074S, RRID:AB_2099233). Bands were developed using ECL Prime western blotting detection reagent (GE Healthcare, RPN2232) and visualized with an autoradiography film (LabScientific, XAR ALF 2025).

Immunomagnetic purification of NK cells and treatment with rIL-27 *in vitro*

NK cells and ILC were enriched from spleen and liver of wild type male mice by negative selection (Stem cell, 19855) followed by antibody staining CD49a-PE (HMα1; BioLegend, 142604, RRID:AB_10945158) and CD49b-PE (DX5; BioLegend, 108908, RRID:AB_313415) and PE-positive selection (Stem Cell, 18755, 17656) using magnetic beads. Purified NK cells were plated at 250,000 cells per well of 12-well plate in complete RPMI-1640 with 5%FBS with or without 25 ng/mL of rIL-27(BioLegend, 577404) for 12h followed by gene expression analysis.

NK cytotoxicity and degranulation assays *in vitro*

NK cells were isolated by negative selection (Stem cell, 19855) from *Il27ra*$^{-/-}$ and *Il27ra*$^{+/-}$ mice and incubated with lymphoblast target cell line YAC-1(RRID: CVCL_2244) in 1:1 ratio at 10,000 per well of 96-well plate in complete RPMI media for 90 min at 37 C. Supernatant was used to assay cytotoxic efficiency of NK cells using CytoTox cell-mediated cytotoxicity assay (Promega, G1780) according to manufacturer's protocol. Absorbance of light was measured at 490 nm. Killing efficiency was calculated as a ratio of experimental values to positive control (lysed target cells).

For degranulation assay, NK cells after the incubation with YAC1 were stained on ice for 30 min with antibodies cocktail: NK1.1-FITC (PK136; BioLegend, 108706), CD49a-Cy7/PE (HMα1; BioLegend, 142608), CD49b-APC (DX5, BioLegend, 108910), CD45-PerCP (30F-11; BioLegend, 103130), TCRβ-Alexa Fluor 700 (H57–597; BioLegend, 109224) and CD107a-PE, [1D4B; BioLegend, 121612, RRID:AB_2134487) and analyzed on BD Aria II flow cytometer. LIVE/DEAD Fixable Yellow Dead Cell stain (Invitrogen, L34959) was used to exclude dead cells. CD107a was used as a marker of degranulation.

NK cytotoxicity *in vivo*

NK cell mediated cytotoxicity was measured as previously described (109). Briefly, RMA (RRID: CVCL_J385) and RMA-S (RRID: CVCL_2180) T-cell lymphoma cells were labeled with Orange CMRA (Invitrogen, C34551) or CPD eFluor 650 (eBioscience, 65–0840-90) dyes, respectively. 2×10^5 cells of each cell line were mixed in a 1:1 ratio and injected i.p. to *Il27ra*$^{+/-}$ or *Il27ra*$^{-/-}$ mice. 48h later mice were sacrificed, peritoneal lavage was collected and analyzed by FACS.

Hydrodynamic Transfection of Murine IL-27 Minicircles

Six-week-old female Balb/c mice were injected with 20 μg of either empty vector or linked murine IL-27 minicircle DNA (System Biosciences, Palo Alto, CA) in 2 ml 0.9% normal saline via the tail vein over the course of 5 sec. Injected animals were transferred to an empty cage with a heating pad to recover for 5 min. Five days post injection mice were injected IP with 1mg SRF381 or isotype control antibodies. Twenty-four hours post antibody treatment whole blood was collected into K2-EDTA tubes and spun for plasma separation.

Minicircle-derived IL-27 pSTAT1 phosphorylation assay

Spleens were isolated from 6–8 week-old female Balb/c mice and single cell suspensions were prepared by mechanical disruption followed by red blood cell lysis in ACK buffer. 3×10^5 splenocytes were incubated with 10μl of plasma collected from IL-27 minicircle-expressing mice for 30 min at 37°C with shaking. Cells were fixed in 5% paraformaldehyde for 5 min at 37°C and then permeabilized with BD permeabilization buffer for 15 min at 4°C. Cells were stained with FITC-conjugated anti-CD3 and PE-conjugated anti-pSTAT1 Y701 for 1 h at RT following by the analysis on a BD LSR Fortessa X20 flow cytometer. pSTAT1+ cells were analyzed in the CD3+ T cell and NK1.1+ populations using FlowJo_V10 Software (Ashland, OR).

Analysis of HCC single cell datasets

Published single cell RNA sequencing dataset (GSE140228 (43)) was analyzed for expression of *IL27RA*, *IL27P28*, and *IL27EBI3* in HCC patients using BBrowser software from BioTuring (110). Published single cell RNA sequencing dataset (GEO125449 (53)), which included HCC cells (n=788) and tumor-associated non-malignant cells (n=2,079) from six HCC patients was analyzed for the impact of HCC *IL27RA* expression on NK cell activation. For HCC cells, we identified their *IL27RA* expression levels which were used to define *IL27RA+* tumor (any cells from the same HCC tumor with positive *IL27RA* expression) and *IL27RA*- tumor. For the non-malignant cells, we first used a collection of markers to exclude T cells (CD2, CD3E, CD3D, CD3G), B cells (CD79A, SLAMF7, BLNK, FCRL5), TECs (PECAM1, VWF, ENG, CDH5), CAFs (COL1A2, FAP, PDPN, DCN, COL3A1, COL6A1), TAMs (CD14, CD163, CD68, CSF1R) and liver cell (EPCAM, KRT19, PROM1, ALDH1A1, CD24). Subsequently, NK cells were identified by positive expression of KLRB1, KLRC3, KLRC4 and KLRD1, and these NK cells were then grouped according the IL27RA status of their originated tumors. Lastly, the activation status of NK cells was estimated by the mean expression of NK cell activation signature used by CIBERSORT(111) and compared between *IL27RA*+ and *IL27RA*- tumors.

Mouse single cell RNA sequencing

$CD45^+NK1.1^+$ and $CD45^+NK1.1^-$ cells from tumor and non-tumor tissue of DEN-treated *Il27ra*$^{-/-}$ and *Il27ra*$^{+/-}$ mice were FACS sorted followed by single cell sorting. The single-cell droplets were generated with chromium single-cell controller using Chromium Next GEM Single Cell 3' Kit v3.1 (10× Genomics, 1000121). Approximately 5,000–10,000 cells were collected to make cDNA at the single-cell level. cDNA was fragmented to ~270 bp and the Illumina adapters with index, barcode, and UMI were ligated to the fragmented cDNA. After PCR, purification, and size selection, the scRNA libraries were ~ 450bp and sequenced on NovaSeq 6000 (Illumina) at Novogene. Fastq files were obtained for the bioinformatic analysis.

Bioinformatic analysis of scRNAseq

Using the 10× Genomics Cell Ranger pipeline, reads were aligned to the mouse genome (mm10), and the sequencing depth was subsampled to about 30,000 reads per cell. Further processing, normalization, batch correction, clustering, differential gene expression analysis,

and visualization were performed using the Seurat package and the ggplot2 package in R. Contaminant cells were identified and removed through combining the NK1.1^{+} and NK1.1^{-} sorted samples, clustering the cells, and classifying the cell type of each cluster. For the combined analysis, cells that have less than 200 or over 3,400 unique genes were filtered, and cells that have over 7% mitochondrial counts were filtered. Contaminant NK1.1-negative cell types were computationally removed from single-cell sequenced NK1.1^{+} sorted samples, and NK1.1-positive cell types were computationally removed from single-cell sequenced NK1.1^{-} sorted samples. Cells that have less than 300 or over 2,400 unique genes were filtered out, and cells that have over 5.5% mitochondrial counts were filtered out as well. Myeloid cell type marker genes were also filtered out from NK1.1^{+} dataset.

For cell type prediction for cluster classification, the total gene expression of each cluster was analyzed using Gene Set Enrichment Analysis (GSEA) and compared to a gmx file containing gene signatures of all cell types that we derived in house from the Immgen database (www.immgen.org) and NK and ILC gene signatures from Robinette et al (57). The GSEA analysis was done in the fgsea package in R (112). Markers that define clusters (found via differential expression analysis), NK and ILC markers from McFarland et al.(52), and other known cell type markers (such as *Cd3*, *Prf1*, and *Gzmb*) were used to supplement this analysis for cell prediction.

For differential gene expression analysis, the Wilcoxon rank sum test was used, and the adjusted p-value was calculated based on Bonferroni correction using all features in the dataset. Cluster markers were identified as differentially expressed genes in each cluster compared to all other clusters among genes that show at least 0.25-fold difference (log-scale) between the two populations and are detected in at least 25% of either of the two populations. When comparing samples, differentially expressed genes were identified among genes that are detected in at least 1% of either of the two populations. Identified differentially expressed genes were passed to DAVID Functional Annotation Bioinformatics Microarray Analysis to search for enriched gene sets. PERMANOVA values were calculated using the adonis function of the vegan package in R, with 10,000 permutations and pairwise distances calculated using Bray-Curtis distance.

For trajectory analysis, the Slingshot package in R was used to create and visualize the trajectories(113). Differential gene expression analysis with the trajectories was performed and visualized using the tradeSeq package in R (114).

Statistical Analysis

Student’s two-tailed t-test was used for comparison between two groups. Survival curve data were analyzed using the long-rank (Mantel-Cox) test. Tukey’s test was used for multiple comparisons. Data were analyzed using the GraphPad Prism Software (Version 7.0). Data are presented as mean ± SEM; *p< 0.05, **p < 0.01, ***p < 0.001, ****p<0.0001. A p-value < 0.05 was considered statistically significant.

Data Availability

The data generated in this study are available upon reasonable request from the corresponding author. ScRNA seq data generated in this study were deposited to Gene Expression Omnibus (GEO) with an accession number GSE200040.

Supplementary Material

Refer to Web version on PubMed Central for supplementary material.

Acknowledgments

We acknowledge the help of FCCC and Cedars-Sinai Medical Center facilities. We thank Dr. Ofer Mandelboim (Hebrew University, Jerusalem) for access to *Ncr1*$^{gfp/gfp}$ mice and Dr. Wayne Yokoyama (Washington University, St. Louis) for providing the mice after backcrossing to the C57BL/6 background and microsatellite mapping verification. We thank Amgen Inc for providing anti-IL-27R antibody. The sera and associated clinical data from patients operated on for HCC were obtained from the Hepatopancreatobiliary Biobank of the Centre hospitalier de l'Université de Montréal, supported by the Université de Montréal Roger Des Groseillers Chair and the Institut du Cancer de Montréal. This work utilized the computational resources of the NIH HPC Biowulf cluster (http://hpc.nih.gov). This work was supported NIH/NCI Cancer Center Support Grant P30 CA006927 to Fox Chase Cancer Center; WW Smith Charitable Trust, NIH R21 CA202396, R01 HL133669 and R01 HL149946 grants to E.K.K. and NIH R01 CA227629 and CA218133 to S.I.G. This work was partially supported by Cedars-Sinai Cancer funds to E.K.K. and S.I.G.. M.H. and X.W.W. were supported by grants (ZIA BC 010877, ZIA BC 010876, ZIA BC 010313 and ZIA BC 011870) from the intramural research program of the Center for Cancer Research, National Cancer Institute of the United States.

K.F.W, M.R., R.M. and J.A.H. are either current or former employees and stockholders of Surface Oncology, Inc. J.S. received research funding and is a scientific advisor and stockholder of Surface Oncology. E.K.K. received research funding from Surface Oncology to investigate IL-27 blockade in HCC. J.A.H., M.R., K.F.W. and E.K.K. are inventors on pending patent applications associated with the topic presented in this article. Other authors declare no potential conflicts of interest.

References:

1. Balogh J, Victor D 3rd, Asham EH, Burroughs SG, Boktour M, Saharia A, et al. Hepatocellular carcinoma: a review. J Hepatocell Carcinoma 2016;3:41–53 doi 10.2147/JHC.S61146. [PubMed: 27785449]
2. Yang JD, Hainaut P, Gores GJ, Amadou A, Plymoth A, Roberts LR. A global view of hepatocellular carcinoma: trends, risk, prevention and management. Nat Rev Gastroenterol Hepatol 2019;16(10):589–604 doi 10.1038/s41575-019-0186-y. [PubMed: 31439937]
3. Roma-Rodrigues C, Mendes R, Baptista PV, Fernandes AR. Targeting Tumor Microenvironment for Cancer Therapy. Int J Mol Sci 2019;20(4) doi 10.3390/ijms20040840.
4. Zhong S, Jeong JH, Chen Z, Chen Z, Luo JL. Targeting Tumor Microenvironment by Small-Molecule Inhibitors. Transl Oncol 2020;13(1):57–69 doi 10.1016/j.tranon.2019.10.001. [PubMed: 31785429]
5. Mahipal A, Tella SH, Kommalapati A, Lim A, Kim R. Immunotherapy in Hepatocellular Carcinoma: Is There a Light at the End of the Tunnel? Cancers (Basel) 2019;11(8) doi 10.3390/cancers11081078.
6. Wang M, Yin B, Wang HY, Wang RF. Current advances in T-cell-based cancer immunotherapy. Immunotherapy 2014;6(12):1265–78 doi 10.2217/imt.14.86. [PubMed: 25524383]
7. Shalapour S, Lin XJ, Bastian IN, Brain J, Burt AD, Aksenov AA, et al. Inflammation-induced IgA+ cells dismantle anti-liver cancer immunity. Nature 2017;551(7680):340–5 doi 10.1038/nature24302. [PubMed: 29144460]
8. El-Serag HB. Epidemiology of viral hepatitis and hepatocellular carcinoma. Gastroenterology 2012;142(6):1264–73 e1 doi 10.1053/j.gastro.2011.12.061. [PubMed: 22537432]

9. Wallace MC, Preen D, Jeffrey GP, Adams LA. The evolving epidemiology of hepatocellular carcinoma: a global perspective. Expert Rev Gastroenterol Hepatol 2015;9(6):765–79 doi 10.1586/17474124.2015.1028363. [PubMed: 25827821]
10. Park EJ, Lee JH, Yu GY, He G, Ali SR, Holzer RG, et al. Dietary and genetic obesity promote liver inflammation and tumorigenesis by enhancing IL-6 and TNF expression. Cell 2010;140(2):197–208 doi 10.1016/j.cell.2009.12.052. [PubMed: 20141834]
11. Schreiber RD, Old LJ, Smyth MJ. Cancer immunoediting: integrating immunity's roles in cancer suppression and promotion. Science 2011;331(6024):1565–70 doi 10.1126/science.1203486. [PubMed: 21436444]
12. Ringelhan M, Pfister D, O'Connor T, Pikarsky E, Heikenwalder M. The immunology of hepatocellular carcinoma. Nat Immunol 2018;19(3):222–32 doi 10.1038/s41590-018-0044-z. [PubMed: 29379119]
13. Lan RY, Salunga TL, Tsuneyama K, Lian ZX, Yang GX, Hsu W, et al. Hepatic IL-17 responses in human and murine primary biliary cirrhosis. J Autoimmun 2009;32(1):43–51 doi 10.1016/j.jaut.2008.11.001. [PubMed: 19101114]
14. Ma S, Cheng Q, Cai Y, Gong H, Wu Y, Yu X, et al. IL-17A produced by gammadelta T cells promotes tumor growth in hepatocellular carcinoma. Cancer research 2014;74(7):1969–82 doi 10.1158/0008-5472.CAN-13-2534. [PubMed: 24525743]
15. Garnelo M, Tan A, Her Z, Yeong J, Lim CJ, Chen J, et al. Interaction between tumour-infiltrating B cells and T cells controls the progression of hepatocellular carcinoma. Gut 2017;66(2):342–51 doi 10.1136/gutjnl-2015-310814. [PubMed: 26669617]
16. Jenne CN, Kubes P. Immune surveillance by the liver. Nat Immunol 2013;14(10):996–1006 doi 10.1038/ni.2691. [PubMed: 24048121]
17. Tian Z, Chen Y, Gao B. Natural killer cells in liver disease. Hepatology 2013;57(4):1654–62 doi 10.1002/hep.26115. [PubMed: 23111952]
18. Cai L, Zhang Z, Zhou L, Wang H, Fu J, Zhang S, et al. Functional impairment in circulating and intrahepatic NK cells and relative mechanism in hepatocellular carcinoma patients. Clin Immunol 2008;129(3):428–37 doi 10.1016/j.clim.2008.08.012. [PubMed: 18824414]
19. Yoshida H, Miyazaki Y. Regulation of immune responses by interleukin-27. Immunological reviews 2008;226:234–47 doi 10.1111/j.1600-065X.2008.00710.x. [PubMed: 19161428]
20. Yoshida H, Hunter CA. The immunobiology of interleukin-27. Annu Rev Immunol 2015;33:417–43 doi 10.1146/annurev-immunol-032414-112134. [PubMed: 25861977]
21. Gao B, Wang H, Lafdil F, Feng D. STAT proteins - key regulators of anti-viral responses, inflammation, and tumorigenesis in the liver. J Hepatol 2012;57(2):430–41 doi 10.1016/j.jhep.2012.01.029. [PubMed: 22504331]
22. Stumhofer JS, Laurence A, Wilson EH, Huang E, Tato CM, Johnson LM, et al. Interleukin 27 negatively regulates the development of interleukin 17-producing T helper cells during chronic inflammation of the central nervous system. Nat Immunol 2006;7(9):937–45 doi ni1376 [pii] 10.1038/ni1376. [PubMed: 16906166]
23. Koltsova EK, Kim G, Lloyd KM, Saris CJ, von Vietinghoff S, Kronenberg M, et al. Interleukin-27 receptor limits atherosclerosis in Ldlr−/− mice. Circulation research 2012;111(10):1274–85 doi 10.1161/CIRCRESAHA.112.277525. [PubMed: 22927332]
24. Hirase T, Hara H, Miyazaki Y, Ide N, Nishimoto-Hazuku A, Fujimoto H, et al. Interleukin 27 inhibits atherosclerosis via immunoregulation of macrophages in mice. American journal of physiology Heart and circulatory physiology 2013;305(3):H420–9 doi 10.1152/ajpheart.00198.2013. [PubMed: 23729211]
25. Sasaoka T, Ito M, Yamashita J, Nakajima K, Tanaka I, Narita M, et al. Treatment with IL-27 attenuates experimental colitis through the suppression of the development of IL-17-producing T helper cells. Am J Physiol Gastrointest Liver Physiol 2011;300(4):G568–76 doi 10.1152/ajpgi.00329.2010. [PubMed: 21193526]
26. Chihara N, Madi A, Kondo T, Zhang H, Acharya N, Singer M, et al. Induction and transcriptional regulation of the co-inhibitory gene module in T cells. Nature 2018;558(7710):454–9 doi 10.1038/s41586-018-0206-z. [PubMed: 29899446]

27. Diveu C, McGeachy MJ, Boniface K, Stumhofer JS, Sathe M, Joyce-Shaikh B, et al. IL-27 blocks RORc expression to inhibit lineage commitment of Th17 cells. J Immunol 2009;182(9):5748–56 doi 182/9/5748 [pii] 10.4049/jimmunol.0801162. [PubMed: 19380822]
28. Huber M, Steinwald V, Guralnik A, Brustle A, Kleemann P, Rosenplanter C, et al. IL-27 inhibits the development of regulatory T cells via STAT3. International immunology 2008;20(2):223–34 doi 10.1093/intimm/dxm139. [PubMed: 18156621]
29. Morishima N, Mizoguchi I, Okumura M, Chiba Y, Xu M, Shimizu M, et al. A pivotal role for interleukin-27 in CD8+ T cell functions and generation of cytotoxic T lymphocytes. J Biomed Biotechnol 2010;2010:605483 doi 10.1155/2010/605483. [PubMed: 20454646]
30. Hunter CA, Kastelein R. Interleukin-27: balancing protective and pathological immunity. Immunity 2012;37(6):960–9 doi 10.1016/j.immuni.2012.11.003. [PubMed: 23244718]
31. Dibra D, Xia X, Mitra A, Cutrera JJ, Lozano G, Li S. Mutant p53 in concert with an interleukin-27 receptor alpha deficiency causes spontaneous liver inflammation, fibrosis, and steatosis in mice. Hepatology 2016;63(3):1000–12 doi 10.1002/hep.28379. [PubMed: 26637970]
32. Salcedo R, Stauffer JK, Lincoln E, Back TC, Hixon JA, Hahn C, et al. IL-27 mediates complete regression of orthotopic primary and metastatic murine neuroblastoma tumors: role for CD8+ T cells. J Immunol 2004;173(12):7170–82. [PubMed: 15585838]
33. Salcedo R, Hixon JA, Stauffer JK, Jalah R, Brooks AD, Khan T, et al. Immunologic and therapeutic synergy of IL-27 and IL-2: enhancement of T cell sensitization, tumor-specific CTL reactivity and complete regression of disseminated neuroblastoma metastases in the liver and bone marrow. J Immunol 2009;182(7):4328–38 doi 10.4049/jimmunol.0800471. [PubMed: 19299733]
34. Natividad KD, Junankar SR, Mohd Redzwan N, Nair R, Wirasinha RC, King C, et al. Interleukin-27 signaling promotes immunity against endogenously arising murine tumors. PLoS One 2013;8(3):e57469 doi 10.1371/journal.pone.0057469. [PubMed: 23554861]
35. Dibra D, Mitra A, Newman M, Xia X, Cutrera JJ, Gagea M, et al. Lack of Immunomodulatory Interleukin-27 Enhances Oncogenic Properties of Mutant p53 In Vivo. Clin Cancer Res 2016;22(15):3876–83 doi 10.1158/1078-0432.CCR-15-2052. [PubMed: 26979394]
36. Villarino A, Hibbert L, Lieberman L, Wilson E, Mak T, Yoshida H, et al. The IL-27R (WSX-1) is required to suppress T cell hyperactivity during infection. Immunity 2003;19(5):645–55 doi S1074761303003005 [pii]. [PubMed: 14614852]
37. Findlay EG, Greig R, Stumhofer JS, Hafalla JC, de Souza JB, Saris CJ, et al. Essential role for IL-27 receptor signaling in prevention of Th1-mediated immunopathology during malaria infection. J Immunol 2010;185(4):2482–92 doi jimmunol.0904019 [pii]10.4049/jimmunol.0904019. [PubMed: 20631310]
38. Fitzgerald DC, Ciric B, Touil T, Harle H, Grammatikopolou J, Das Sarma J, et al. Suppressive effect of IL-27 on encephalitogenic Th17 cells and the effector phase of experimental autoimmune encephalomyelitis. Journal of immunology 2007;179(5):3268–75.
39. Peshkova IO, Fatkhullina AR, Mikulski Z, Ley K, Koltsova EK. IL-27R signaling controls myeloid cells accumulation and antigen-presentation in atherosclerosis. Sci Rep 2017;7(1):2255 doi 10.1038/s41598-017-01828-8. [PubMed: 28536468]
40. Peshkova IO, Aghayev T, Fatkhullina AR, Makhov P, Titerina EK, Eguchi S, et al. IL-27 receptor-regulated stress myelopoiesis drives abdominal aortic aneurysm development. Nat Commun 2019;10(1):5046 doi 10.1038/s41467-019-13017-4. [PubMed: 31695038]
41. Woo HG, Lee JH, Yoon JH, Kim CY, Lee HS, Jang JJ, et al. Identification of a cholangiocarcinoma-like gene expression trait in hepatocellular carcinoma. Cancer Res 2010;70(8):3034–41 doi 10.1158/0008-5472.CAN-09-2823. [PubMed: 20395200]
42. Roessler S, Jia HL, Budhu A, Forgues M, Ye QH, Lee JS, et al. A unique metastasis gene signature enables prediction of tumor relapse in early-stage hepatocellular carcinoma patients. Cancer Res 2010;70(24):10202–12 doi 10.1158/0008-5472.CAN-10-2607. [PubMed: 21159642]
43. Zhang Q, He Y, Luo N, Patel SJ, Han Y, Gao R, et al. Landscape and Dynamics of Single Immune Cells in Hepatocellular Carcinoma. Cell 2019;179(4):829–45 e20 doi 10.1016/j.cell.2019.10.003. [PubMed: 31675496]

44. Naugler WE, Sakurai T, Kim S, Maeda S, Kim K, Elsharkawy AM, et al. Gender disparity in liver cancer due to sex differences in MyD88-dependent IL-6 production. Science 2007;317(5834):121–4 doi 10.1126/science.1140485. [PubMed: 17615358]
45. Sakurai T, He G, Matsuzawa A, Yu GY, Maeda S, Hardiman G, et al. Hepatocyte necrosis induced by oxidative stress and IL-1 alpha release mediate carcinogen-induced compensatory proliferation and liver tumorigenesis. Cancer Cell 2008;14(2):156–65 doi 10.1016/j.ccr.2008.06.016. [PubMed: 18691550]
46. Bakiri L, Wagner EF. Mouse models for liver cancer. Molecular oncology 2013;7(2):206–23 doi 10.1016/j.molonc.2013.01.005. [PubMed: 23428636]
47. Ranson T, Vosshenrich CA, Corcuff E, Richard O, Muller W, Di Santo JP. IL-15 is an essential mediator of peripheral NK-cell homeostasis. Blood 2003;101(12):4887–93 doi 10.1182/blood-2002-11-3392. [PubMed: 12586624]
48. Marcais A, Viel S, Grau M, Henry T, Marvel J, Walzer T. Regulation of mouse NK cell development and function by cytokines. Front Immunol 2013;4:450 doi 10.3389/fimmu.2013.00450. [PubMed: 24376448]
49. Crinier A, Kerdiles Y, Vienne M, Cozar B, Vivier E, Berruyer C. Multidimensional molecular controls defining NK/ILC1 identity in cancers. Semin Immunol 2021;52:101424 doi 10.1016/j.smim.2020.101424. [PubMed: 33272899]
50. Vivier E, Artis D, Colonna M, Diefenbach A, Di Santo JP, Eberl G, et al. Innate Lymphoid Cells: 10 Years On. Cell 2018;174(5):1054–66 doi 10.1016/j.cell.2018.07.017. [PubMed: 30142344]
51. O'Sullivan TE. Dazed and Confused: NK Cells. Front Immunol 2019;10:2235 doi 10.3389/fimmu.2019.02235. [PubMed: 31616419]
52. McFarland AP, Yalin A, Wang SY, Cortez VS, Landsberger T, Sudan R, et al. Multi-tissue single-cell analysis deconstructs the complex programs of mouse natural killer and type 1 innate lymphoid cells in tissues and circulation. Immunity 2021;54(6):1320–37 e4 doi 10.1016/j.immuni.2021.03.024. [PubMed: 33945787]
53. Ma L, Hernandez MO, Zhao Y, Mehta M, Tran B, Kelly M, et al. Tumor Cell Biodiversity Drives Microenvironmental Reprogramming in Liver Cancer. Cancer Cell 2019;36(4):418–30 e6 doi 10.1016/j.ccell.2019.08.007. [PubMed: 31588021]
54. Stegmann KA, Robertson F, Hansi N, Gill U, Pallant C, Christophides T, et al. CXCR6 marks a novel subset of T-bet(lo)Eomes(hi) natural killer cells residing in human liver. Sci Rep 2016;6:26157 doi 10.1038/srep26157. [PubMed: 27210614]
55. Hudspeth K, Donadon M, Cimino M, Pontarini E, Tentorio P, Preti M, et al. Human liver-resident CD56(bright)/CD16(neg) NK cells are retained within hepatic sinusoids via the engagement of CCR5 and CXCR6 pathways. J Autoimmun 2016;66:40–50 doi 10.1016/j.jaut.2015.08.011. [PubMed: 26330348]
56. Hao Y, Hao S, Andersen-Nissen E, Mauck WM 3rd, Zheng S, Butler A, et al. Integrated analysis of multimodal single-cell data. Cell 2021;184(13):3573–87 e29 doi 10.1016/j.cell.2021.04.048. [PubMed: 34062119]
57. Robinette ML, Fuchs A, Cortez VS, Lee JS, Wang Y, Durum SK, et al. Transcriptional programs define molecular characteristics of innate lymphoid cell classes and subsets. Nat Immunol 2015;16(3):306–17 doi 10.1038/ni.3094. [PubMed: 25621825]
58. O'Brien KL, Finlay DK. Immunometabolism and natural killer cell responses. Nat Rev Immunol 2019;19(5):282–90 doi 10.1038/s41577-019-0139-2. [PubMed: 30808985]
59. Assmann N, O'Brien KL, Donnelly RP, Dyck L, Zaiatz-Bittencourt V, Loftus RM, et al. Srebp-controlled glucose metabolism is essential for NK cell functional responses. Nat Immunol 2017;18(11):1197–206 doi 10.1038/ni.3838. [PubMed: 28920951]
60. Maul-Pavicic A, Chiang SC, Rensing-Ehl A, Jessen B, Fauriat C, Wood SM, et al. ORAI1-mediated calcium influx is required for human cytotoxic lymphocyte degranulation and target cell lysis. Proc Natl Acad Sci U S A 2011;108(8):3324–9 doi 10.1073/pnas.1013285108. [PubMed: 21300876]
61. Ward-Kavanagh LK, Lin WW, Sedy JR, Ware CF. The TNF Receptor Superfamily in Co-stimulating and Co-inhibitory Responses. Immunity 2016;44(5):1005–19 doi 10.1016/j.immuni.2016.04.019. [PubMed: 27192566]

62. Adams NM, Lau CM, Fan X, Rapp M, Geary CD, Weizman OE, et al. Transcription Factor IRF8 Orchestrates the Adaptive Natural Killer Cell Response. Immunity 2018;48(6):1172–82 e6 doi 10.1016/j.immuni.2018.04.018. [PubMed: 29858012]

63. Crinier A, Milpied P, Escaliere B, Piperoglou C, Galluso J, Balsamo A, et al. High-Dimensional Single-Cell Analysis Identifies Organ-Specific Signatures and Conserved NK Cell Subsets in Humans and Mice. Immunity 2018;49(5):971–86 e5 doi 10.1016/j.immuni.2018.09.009. [PubMed: 30413361]

64. Park KU, Jin P, Sabatino M, Feng J, Civini S, Khuu H, et al. Gene expression analysis of ex vivo expanded and freshly isolated NK cells from cancer patients. J Immunother 2010;33(9):945–55 doi 10.1097/CJI.0b013e3181f71b81. [PubMed: 20948442]

65. Friedrich C, Taggenbrock R, Doucet-Ladeveze R, Golda G, Moenius R, Arampatzi P, et al. Effector differentiation downstream of lineage commitment in ILC1s is driven by Hobit across tissues. Nat Immunol 2021;22(10):1256–67 doi 10.1038/s41590-021-01013-0. [PubMed: 34462601]

66. Long EO, Kim HS, Liu D, Peterson ME, Rajagopalan S. Controlling natural killer cell responses: integration of signals for activation and inhibition. Annu Rev Immunol 2013;31:227–58 doi 10.1146/annurev-immunol-020711-075005. [PubMed: 23516982]

67. Phillips LK, Gould EA, Babu H, Krams SM, Palmer TD, Martinez OM. Natural killer cell-activating receptor NKG2D mediates innate immune targeting of allogeneic neural progenitor cell grafts. Stem Cells 2013;31(9):1829–39 doi 10.1002/stem.1422. [PubMed: 23733329]

68. Zhu J, Huang X, Yang Y. NKG2D is required for NK cell activation and function in response to E1-deleted adenovirus. J Immunol 2010;185(12):7480–6 doi 10.4049/jimmunol.1002771. [PubMed: 21076062]

69. Shi L, Li K, Guo Y, Banerjee A, Wang Q, Lorenz UM, et al. Modulation of NKG2D, NKp46, and Ly49C/I facilitates natural killer cell-mediated control of lung cancer. Proc Natl Acad Sci U S A 2018;115(46):11808–13 doi 10.1073/pnas.1804931115. [PubMed: 30381460]

70. Lunemann S, Langeneckert AE, Martrus G, Hess LU, Salzberger W, Ziegler AE, et al. Human liver-derived CXCR6(+) NK cells are predominantly educated through NKG2A and show reduced cytokine production. J Leukoc Biol 2019;105(6):1331–40 doi 10.1002/JLB.1MA1118-428R. [PubMed: 30779432]

71. Long EO. Negative signaling by inhibitory receptors: the NK cell paradigm. Immunol Rev 2008;224:70–84 doi 10.1111/j.1600-065X.2008.00660.x. [PubMed: 18759921]

72. Choi T, Ferris ST, Matsumoto N, Poursine-Laurent J, Yokoyama WM. Ly49-dependent NK cell licensing and effector inhibition involve the same interaction site on MHC ligands. J Immunol 2011;186(7):3911–7 doi 10.4049/jimmunol.1004168. [PubMed: 21335486]

73. Hayakawa Y, Smyth MJ. CD27 dissects mature NK cells into two subsets with distinct responsiveness and migratory capacity. J Immunol 2006;176(3):1517–24 doi 10.4049/jimmunol.176.3.1517. [PubMed: 16424180]

74. Raulet DH, Gasser S, Gowen BG, Deng W, Jung H. Regulation of ligands for the NKG2D activating receptor. Annu Rev Immunol 2013;31:413–41 doi 10.1146/annurev-immunol-032712-095951. [PubMed: 23298206]

75. Molfetta R, Quatrini L, Santoni A, Paolini R. Regulation of NKG2D-Dependent NK Cell Functions: The Yin and the Yang of Receptor Endocytosis. Int J Mol Sci 2017;18(8) doi 10.3390/ijms18081677.

76. Shifrin N, Raulet DH, Ardolino M. NK cell self tolerance, responsiveness and missing self recognition. Semin Immunol 2014;26(2):138–44 doi 10.1016/j.smim.2014.02.007. [PubMed: 24629893]

77. Zamor PJ, deLemos AS, Russo MW. Viral hepatitis and hepatocellular carcinoma: etiology and management. J Gastrointest Oncol 2017;8(2):229–42 doi 10.21037/jgo.2017.03.14. [PubMed: 28480063]

78. Gupta A, Das A, Majumder K, Arora N, Mayo HG, Singh PP, et al. Obesity is Independently Associated With Increased Risk of Hepatocellular Cancer-related Mortality: A Systematic Review and Meta-Analysis. Am J Clin Oncol 2018;41(9):874–81 doi 10.1097/COC.0000000000000388. [PubMed: 28537989]

79. Younossi ZM. Non-alcoholic fatty liver disease - A global public health perspective. J Hepatol 2019;70(3):531–44 doi 10.1016/j.jhep.2018.10.033. [PubMed: 30414863]
80. Febbraio MA, Reibe S, Shalapour S, Ooi GJ, Watt MJ, Karin M. Preclinical Models for Studying NASH-Driven HCC: How Useful Are They? Cell Metab 2019;29(1):18–26 doi 10.1016/j.cmet.2018.10.012. [PubMed: 30449681]
81. Nakagawa H, Umemura A, Taniguchi K, Font-Burgada J, Dhar D, Ogata H, et al. ER stress cooperates with hypernutrition to trigger TNF-dependent spontaneous HCC development. Cancer Cell 2014;26(3):331–43 doi 10.1016/j.ccr.2014.07.001. [PubMed: 25132496]
82. Nakagawa H Recent advances in mouse models of obesity- and nonalcoholic steatohepatitis-associated hepatocarcinogenesis. World J Hepatol 2015;7(17):2110–8 doi 10.4254/wjh.v7.i17.2110. [PubMed: 26301053]
83. Stal P Liver fibrosis in non-alcoholic fatty liver disease - diagnostic challenge with prognostic significance. World J Gastroenterol 2015;21(39):11077–87 doi 10.3748/wjg.v21.i39.11077. [PubMed: 26494963]
84. Xiong X, Kuang H, Ansari S, Liu T, Gong J, Wang S, et al. Landscape of Intercellular Crosstalk in Healthy and NASH Liver Revealed by Single-Cell Secretome Gene Analysis. Mol Cell 2019;75(3):644–60 e5 doi 10.1016/j.molcel.2019.07.028. [PubMed: 31398325]
85. Barrow AD, Martin CJ, Colonna M. The Natural Cytotoxicity Receptors in Health and Disease. Front Immunol 2019;10:909 doi 10.3389/fimmu.2019.00909. [PubMed: 31134055]
86. Gazit R, Gruda R, Elboim M, Arnon TI, Katz G, Achdout H, et al. Lethal influenza infection in the absence of the natural killer cell receptor gene Ncr1. Nat Immunol 2006;7(5):517–23 doi 10.1038/ni1322. [PubMed: 16565719]
87. Wang Y, Dong W, Zhang Y, Caligiuri MA, Yu J. Dependence of innate lymphoid cell 1 development on NKp46. PLoS Biol 2018;16(4):e2004867 doi 10.1371/journal.pbio.2004867. [PubMed: 29702643]
88. Ferlay J, Colombet M, Soerjomataram I, Mathers C, Parkin DM, Pineros M, et al. Estimating the global cancer incidence and mortality in 2018: GLOBOCAN sources and methods. Int J Cancer 2019;144(8):1941–53 doi 10.1002/ijc.31937. [PubMed: 30350310]
89. Yoshida H, Hamano S, Senaldi G, Covey T, Faggioni R, Mu S, et al. WSX-1 is required for the initiation of Th1 responses and resistance to L. major infection. Immunity 2001;15(4):569–78. [PubMed: 11672539]
90. Carl JW, Bai XF. IL27: its roles in the induction and inhibition of inflammation. Int J Clin Exp Pathol 2008;1(2):117–23. [PubMed: 18784808]
91. Yuan JM, Wang Y, Wang R, Luu HN, Adams-Haduch J, Koh WP, et al. Serum IL27 in Relation to Risk of Hepatocellular Carcinoma in Two Nested Case-Control Studies. Cancer Epidemiol Biomarkers Prev 2021;30(2):388–95 doi 10.1158/1055-9965.EPI-20-1081. [PubMed: 33203693]
92. Michelet X, Dyck L, Hogan A, Loftus RM, Duquette D, Wei K, et al. Metabolic reprogramming of natural killer cells in obesity limits antitumor responses. Nat Immunol 2018;19(12):1330–40 doi 10.1038/s41590-018-0251-7. [PubMed: 30420624]
93. Wolf MJ, Adili A, Piotrowitz K, Abdullah Z, Boege Y, Stemmer K, et al. Metabolic Activation of Intrahepatic CD8(+) T Cells and NKT Cells Causes Nonalcoholic Steatohepatitis and Liver Cancer via Cross-Talk with Hepatocytes. Cancer Cell 2014;26(4):549–64 doi 10.1016/j.ccell.2014.09.003. [PubMed: 25314080]
94. Mossanen JC, Kohlhepp M, Wehr A, Krenkel O, Liepelt A, Roeth AA, et al. CXCR6 Inhibits Hepatocarcinogenesis by Promoting Natural Killer T− and CD4(+) T-Cell-Dependent Control of Senescence. Gastroenterology 2019;156(6):1877–89 e4 doi 10.1053/j.gastro.2019.01.247. [PubMed: 30710528]
95. Ma C, Han M, Heinrich B, Fu Q, Zhang Q, Sandhu M, et al. Gut microbiome-mediated bile acid metabolism regulates liver cancer via NKT cells. Science 2018;360(6391) doi 10.1126/science.aan5931.
96. Pflanz S, Timans JC, Cheung J, Rosales R, Kanzler H, Gilbert J, et al. IL-27, a heterodimeric cytokine composed of EBI3 and p28 protein, induces proliferation of naive CD4+ T cells. Immunity 2002;16(6):779–90 doi 10.1016/s1074-7613(02)00324-2. [PubMed: 12121660]

97. Kumar P, Rajasekaran K, Nanbakhsh A, Gorski J, Thakar MS, Malarkannan S. IL-27 promotes NK cell effector functions via Maf-Nrf2 pathway during influenza infection. Sci Rep 2019;9(1):4984 doi 10.1038/s41598-019-41478-6. [PubMed: 30899058]

98. Wu M, Xia X, Hu J, Fowlkes NW, Li S. WSX1 act as a tumor suppressor in hepatocellular carcinoma by downregulating neoplastic PD-L1 expression. Nat Commun 2021;12(1):3500 doi 10.1038/s41467-021-23864-9. [PubMed: 34108491]

99. Han C, Jiang Y, Wang Z, Wang H. Natural killer cells involved in tumour immune escape of hepatocellular carcinomar. Int Immunopharmacol 2019;73:10–6 doi 10.1016/j.intimp.2019.04.057. [PubMed: 31078921]

100. Papatheodoridi AM, Chrysavgis L, Koutsilieris M, Chatzigeorgiou A. The Role of Senescence in the Development of Nonalcoholic Fatty Liver Disease and Progression to Nonalcoholic Steatohepatitis. Hepatology 2020;71(1):363–74 doi 10.1002/hep.30834. [PubMed: 31230380]

101. Pereira BI, Devine OP, Vukmanovic-Stejic M, Chambers ES, Subramanian P, Patel N, et al. Senescent cells evade immune clearance via HLA-E-mediated NK and CD8(+) T cell inhibition. Nat Commun 2019;10(1):2387 doi 10.1038/s41467-019-10335-5. [PubMed: 31160572]

102. Ruscetti M, Leibold J, Bott MJ, Fennell M, Kulick A, Salgado NR, et al. NK cell-mediated cytotoxicity contributes to tumor control by a cytostatic drug combination. Science 2018;362(6421):1416–22 doi 10.1126/science.aas9090. [PubMed: 30573629]

103. Devergne O, Coulomb-L'Hermine A, Capel F, Moussa M, Capron F. Expression of Epstein-Barr virus-induced gene 3, an interleukin-12 p40-related molecule, throughout human pregnancy: involvement of syncytiotrophoblasts and extravillous trophoblasts. Am J Pathol 2001;159(5):1763–76 doi 10.1016/S0002-9440(10)63023-4. [PubMed: 11696437]

104. Weglarz TC, Degen JL, Sandgren EP. Hepatocyte transplantation into diseased mouse liver. Kinetics of parenchymal repopulation and identification of the proliferative capacity of tetraploid and octaploid hepatocytes. Am J Pathol 2000;157(6):1963–74 doi 10.1016/S0002-9440(10)64835-3. [PubMed: 11106569]

105. Zhang Y, Parmigiani G, Johnson WE. ComBat-seq: batch effect adjustment for RNA-seq count data. NAR Genom Bioinform 2020;2(3):lqaa078 doi 10.1093/nargab/lqaa078. [PubMed: 33015620]

106. Mootha VK, Lindgren CM, Eriksson KF, Subramanian A, Sihag S, Lehar J, et al. PGC-1alpha-responsive genes involved in oxidative phosphorylation are coordinately downregulated in human diabetes. Nat Genet 2003;34(3):267–73 doi 10.1038/ng1180. [PubMed: 12808457]

107. Subramanian A, Tamayo P, Mootha VK, Mukherjee S, Ebert BL, Gillette MA, et al. Gene set enrichment analysis: a knowledge-based approach for interpreting genome-wide expression profiles. Proc Natl Acad Sci U S A 2005;102(43):15545–50 doi 10.1073/pnas.0506580102. [PubMed: 16199517]

108. Mitchell C, Willenbring H. A reproducible and well-tolerated method for 2/3 partial hepatectomy in mice. Nat Protoc 2008;3(7):1167–70 doi 10.1038/nprot.2008.80. [PubMed: 18600221]

109. Saudemont A, Burke S, Colucci F. A simple method to measure NK cell cytotoxicity in vivo. Methods Mol Biol 2010;612:325–34 doi 10.1007/978-1-60761-362-6_22. [PubMed: 20033651]

110. Le TP T; Pham M; Tran D; Lam L; Nguyen T; Truong T; Vuong H; Luu T; Phung N; Pham N; Nguyen T; Pham O; Nguyen A; Nguyen H; Tran H; Tran L; Nguyen HA; Tran T; Nguyen N; Tran N; Boysen C; Nguyen U; Pham V; Kim T; Pham N; Gill T; Pham S BBrowser: Making single-cell data easily accessible. bioRxiv 2020 doi 10.1101/2020.12.11.414136

111. Newman AM, Liu CL, Green MR, Gentles AJ, Feng W, Xu Y, et al. Robust enumeration of cell subsets from tissue expression profiles. Nat Methods 2015;12(5):453–7 doi 10.1038/nmeth.3337. [PubMed: 25822800]

112. Sergushichev AA. An algorithm for fast preranked gene set enrichment analysis using cumulative statistic calculation. bioRxiv 2016 doi 10.1101/060012.

113. Street K, Risso D, Fletcher RB, Das D, Ngai J, Yosef N, et al. Slingshot: cell lineage and pseudotime inference for single-cell transcriptomics. BMC Genomics 2018;19(1):477 doi 10.1186/s12864-018-4772-0. [PubMed: 29914354]

114. Van den Berge K, Roux de Bezieux H, Street K, Saelens W, Cannoodt R, Saeys Y, et al. Trajectory-based differential expression analysis for single-cell sequencing data. Nat Commun 2020;11(1):1201 doi 10.1038/s41467-020-14766-3. [PubMed: 32139671]

Significance.

Hepatocellular carcinoma (HCC), the most common form of liver cancer, is characterized by poor survival rate and limited treatment options. The discovery of a novel IL-27-dependent mechanism controlling anti-cancer cytotoxic immune response will pave the road for new treatment options for this devastating disease.

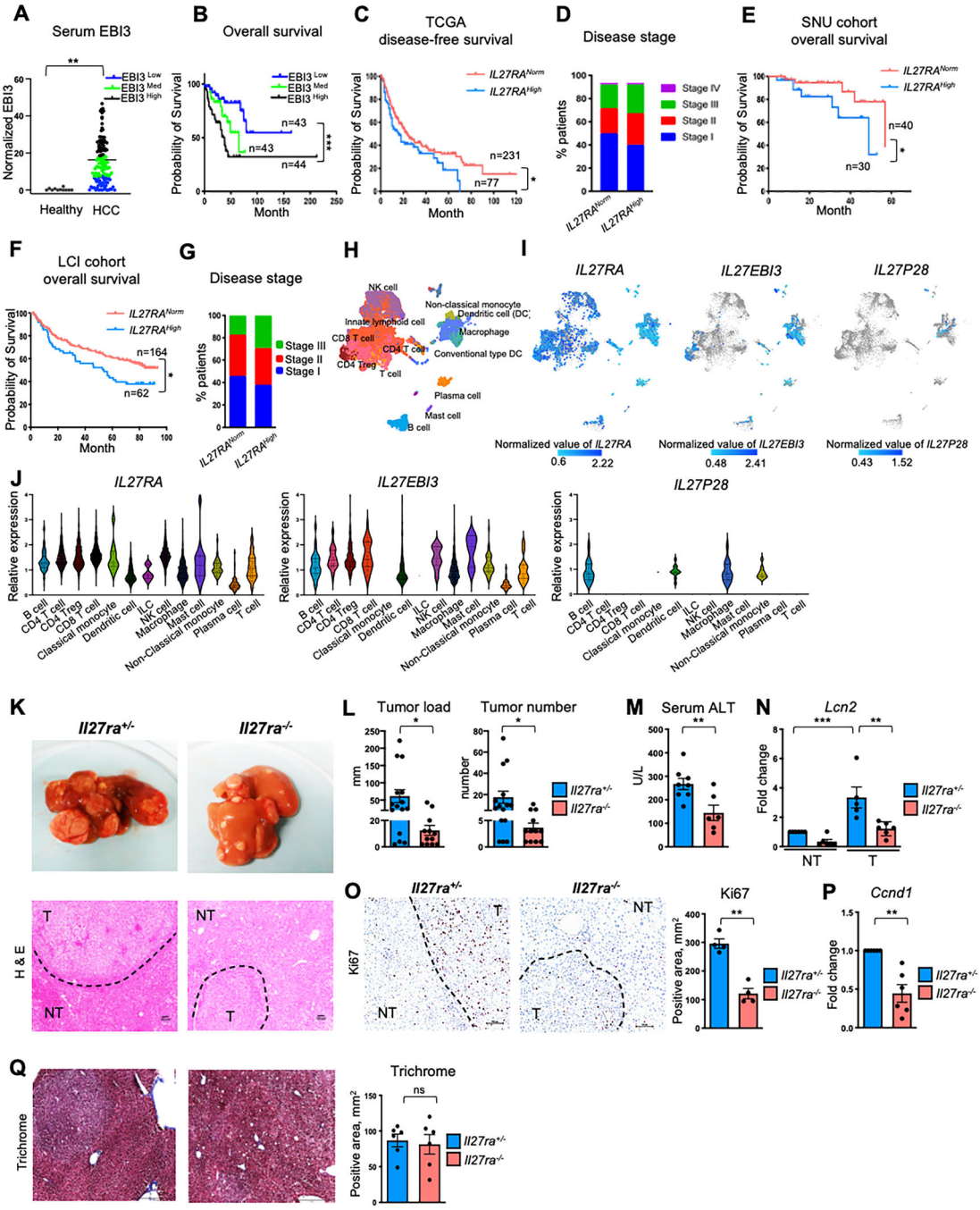

Figure 1. IL-27 signaling regulates liver cancer development.

A, Serum EBI3 levels in healthy controls (n=11, mean EBI3 level=0.36) and HCC patients (n=130, mean EBI3 level=16.33, CHUM cohort). **B,** Correlation between serum EBI3 level and overall survival of 130 HCC patients from CHUM cohort. Overall survival curves were generated based on serum EBI3 levels and separated by tertiles. Statistics were calculated by log-rank test: EBI3 med, hazard ratio (95% CI) = 2.25 (0.93–5.45), p value=0.047; EBI3 high, hazard ratio (95% CI) = 3.69 (1.82–7.47), p value = 0.0002. **C,** TCGA provisional data on disease-free Kaplan-Meier estimate (disease free status since initial treatment) relative

to *IL27RA* expression in HCC tumors. Top 25% expression cutoff (*IL27RA* "high") and lower 75% expression (*IL27RA* "norm") were used to define correlation between *IL27RA* expression in the tumors and disease free survival. **D,** The distribution of clinical stage upon diagnosis among patients with "high"- and "norm"-*IL27RA* expression in TCGA cohort. **E,F,** Kaplan-Meier survival analysis of 70 HCC patients in SNU cohort (GSE15765) **(E)** and 226 HCC patients in LCI cohort (GSE14520) **(F)** based on tumor *IL27RA* expression status with two-sided log rank p-value. For SNU cohort ROC curve analysis with Youden index was used to identify the best cutoff value of *IL27RA* associates with overall survival and this value was used to define "high" (higher expression)- and "norm" (lower expression)-*IL27RA* tumor. For LCI cohort, *IL27RA* expression of tumor tissue was compared to its paired non-tumor tissue, and tumors with the top 25% of *IL27RA* tumor-to-non-tumor ratio were defined as "high" *IL27RA* tumors. **G,** The distribution of clinical stage upon diagnosis among patients with "high"- and "norm"-*IL27RA* expression in the LCI cohort. **H,** Single Cell RNA seq analysis of sorted $CD45^+$ cells from human HCC using 10× Genomics platform. UMAP plot is presented. Annotations are derived from cluster specific analysis (Zhang et al. *Cell* 2019 (43)). **I,** UMAP plots of cell type specific expression pattern for *IL27RA, IL27EBI3* and *IL27P28* among $CD45^+$ clusters from human HCC shown in H. **J,** Violin plots of *IL27RA*, *IL27EBI3*, *IL27P28* expression among clusters. **K,** $Il27ra^{+/-}$ and $Il27ra^{-/-}$ mice received DEN at postnatal day 15. HCC development was analyzed at 10 months of age. Representative images of macroscopic and microscopic views of tumor bearing livers. **L,** Tumor load and tumor number in $Il27ra^{+/-}$ (n=15) and $Il27ra^{-/-}$ (n=12) mice. **M,** Concentration of ALT in sera from $Il27ra^{+/-}$ (n=8) and $Il27ra^{-/-}$ (n=6) tumor-bearing 10-month-old mice. **N,** Relative gene expression of inflammatory marker *Lcn2* in non-tumor and tumor tissues from $Il27ra^{+/-}$ (n=5) and $Il27ra^{-/-}$ (n=6) mice. **O,** Representative images and quantification of Ki67 staining of HCC sections from DEN-treated $Il27ra^{+/-}$ (n=4) and $Il27ra^{-/-}$ (n=4) mice. **P,** Relative gene expression of proliferation marker Cyclin D (*Ccnd1)* in tumors from $Il27ra^{+/-}$ (n=6) and $Il27ra^{-/-}$ (n=6) mice. **Q,** Representative images and quantification of Trichrome staining of HCC sections from DEN-treated $Il27ra^{+/-}$ (n=6) and $Il27ra^{-/-}$ (n=6) mice. For relative gene expression it was first normalized to *Rpl32* then to gene expression in tumors from $Il27ra^{+/-}$ mice. Data are mean ± SEM from at least 3 independent experiments. *p<0.05, **p<0.01, ***p<0.001, unpaired Student's t-test (two-tailed); **p<0.01, ***p<0.001, Tukey's multiple comparisons test.

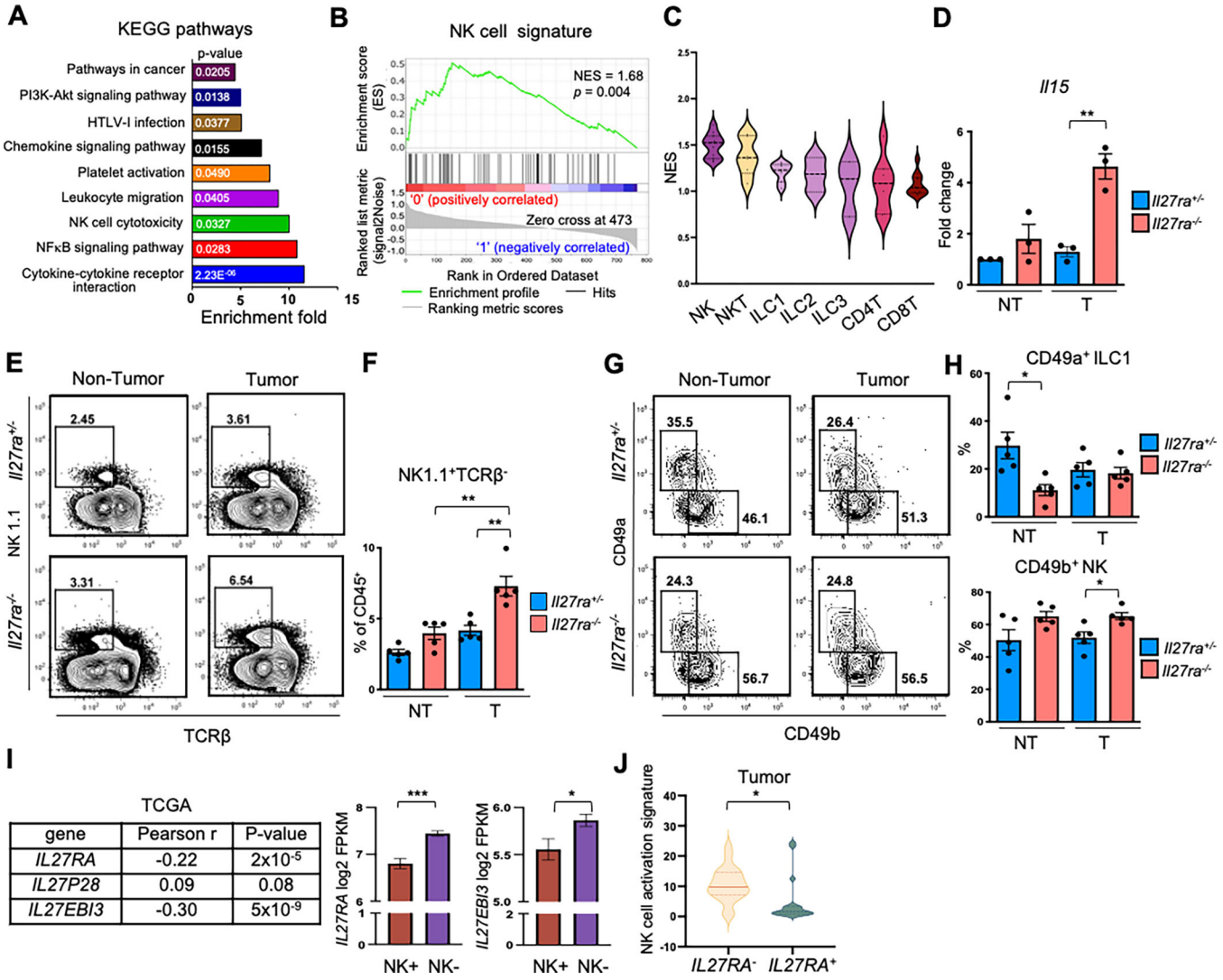

Figure 2. IL-27R signaling regulates NK cell accumulation and function in HCC.

A-C, Differential gene expression analysis of HCC tumors from DEN-treated *Il27ra*$^{+/-}$ (n=6) and *Il27ra*$^{-/-}$ (n=6) mice as determined by NanoString, Cancer Immunopanel, ($p<0.05$). **A,** KEGG pathway analysis of differentially expressed genes. **B,** GSEA enrichment plots for NK genes signatures in tumor of DEN-treated *Il27ra*$^{-/-}$ mice compared to *Il27ra*$^{+/-}$ controls. **C,** Violin plot for enrichment of subset-specific gene expression in tumors from *Il27ra*$^{-/-}$ mice (see Methods for details). **D,** *Il15* gene expression in non-tumor (NT) and tumor (T) tissue as determined by Q-RT-PCR. Gene expression was first normalized to *Rpl32* then to gene expression in non-tumor tissue from *Il27ra*$^{+/-}$ mice. **p<0.01, unpaired Student's t-test (two-tailed). Single cell suspensions of non-tumor and tumor tissues from *Il27ra*$^{+/-}$ (n=5) and *Il27ra*$^{-/-}$ (n=5). DEN-injected 10-month-old mice were stained for Live/Dead, CD45, TCRβ, NK1.1, CD49a and CD49b analyzed by FACS. **E,F,** Representative FACS plots **(E)** and quantified percentage of NK1.1^{+} TCRβ $^{-}$ cells in CD45^{+} gate **(F);** and **G, H,** CD49a^{+}NK1.1^{+} and CD49b^{+}NK1.1^{+} cells in NK1.1^{+}TCRβ $^{-}$gate in NT and T tissues of DEN-treated *Il27ra*$^{+/-}$ (n=5) and *Il27ra*$^{-/-}$ (n=5) mice. Data

are mean ± SEM from at least 2 independent experiments. **I,** Correlation between presence of NK cells in tumors and *IL27RA*, *IL27EBI3*, *IL27P28* expression in TCGA HCC cohort. Expression of *IL27RA* or *IL27EBI3* in tumors with "high" abundance of NK cells (NK+) (n=100); or low abundance of NK cells (NK−) (n=269) as determined by CIBERSORT. **J,** Correlation of activated NK cell signature with *IL27RA* expression in scRNA seq of human HCC (GSE151530; Ma et al. *Cancer Cell*, 2019, (53)).

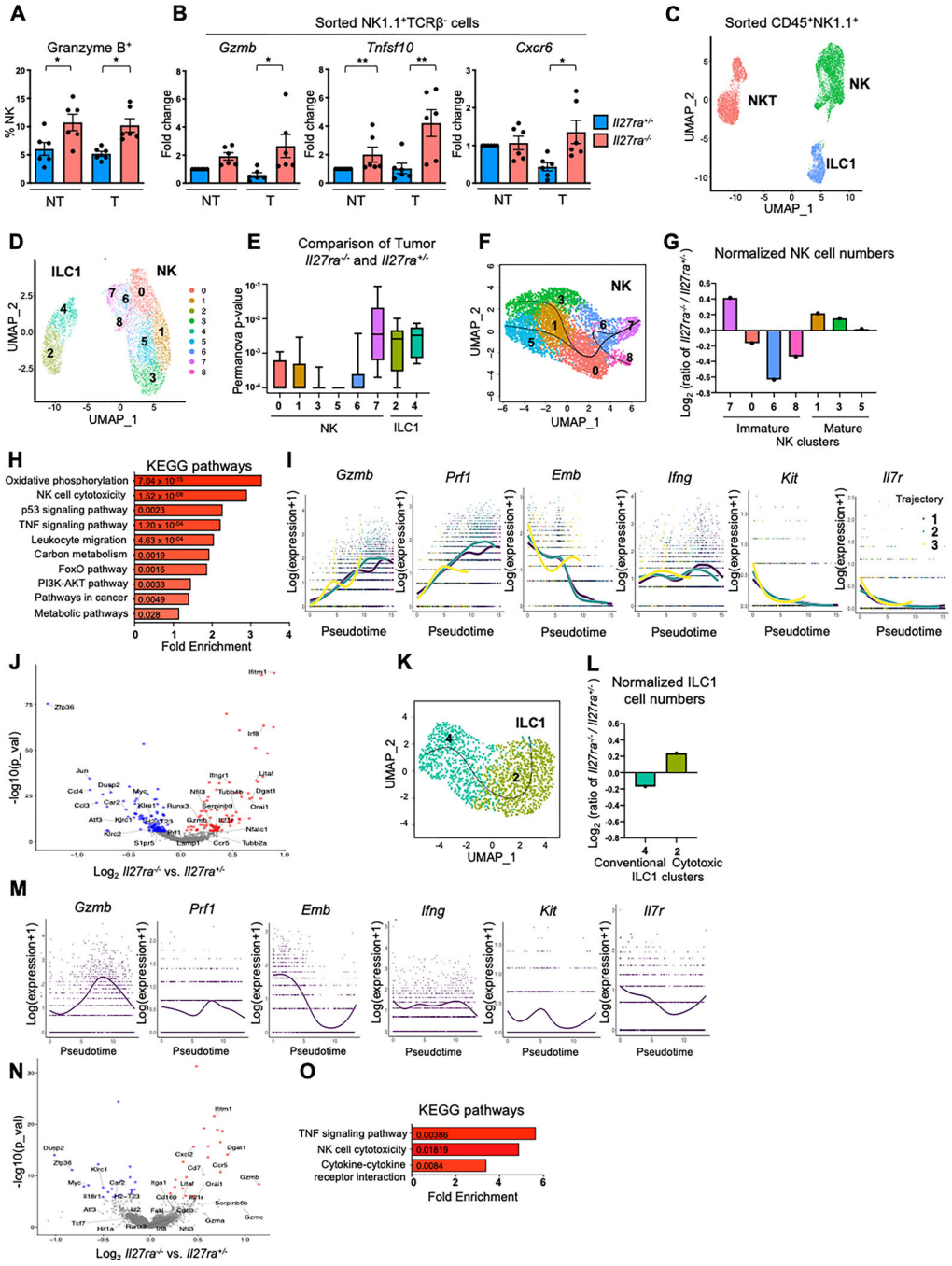

Figure 3. IL-27R signaling regulates activation and cytotoxicity of innate cytotoxic cells.

A, FACS analysis for Granzyme B expression in NK1.1^{+}TCRβ^{-} cells in NT and T tissues from *Il27ra*$^{+/-}$ and *Il27ra*$^{-/-}$ mice (n=6). **B,** Q-RT-PCR analysis of relative gene expression for *Gzmb, Trnsf10* and *Cxcr6* in NK1.1^{+}TCRβ $^{-}$ FACS-sorted cells from non-tumor and tumor tissue of *Il27ra*$^{+/-}$ and *Il27ra*$^{-/-}$ mice (n=6). Gene expression was first normalized to *Rpl32* then to gene expression of NK cells in non-tumor tissue from *Il27ra*$^{+/-}$ mice. Data are mean ± SEM from at least 3 independent experiments. *p<0.05. **p<0.01, Tukey's multiple comparisons test. **C-O,** Non-tumor and tumor tissue from DEN-treated

Il27ra$^{+/-}$ *and Il27ra*$^{-/-}$ mice were dissociated into single cell suspension and FACS sorted for CD45^{+}NK1.1^{+} and applied for 10× Genomics Chromium droplet platform for cell isolation and sequencing. Cells were clustered by differential gene expression. **C,** UMAP of 9511 sorted CD45^{+}NK1.1^{+} cells with identified clusters. **D,** UMAP of ILC1 and NK cells clusters. **E,** Permanova p-value plot of differential gene expression between *Il27ra*$^{+/-}$ and *Il27ra*$^{-/-}$ among clusters of tumor ILC1 and NK cells. **F,** Slingshot trajectory analysis for NK cell clusters. **G,** Normalized cell numbers representing upregulated and downregulated clusters among NK cells in *Il27ra*$^{-/-}$ versus *Il27ra*$^{+/-}$. **H,** KEGG pathway analysis of differentially expressed genes along the trajectory of NK clusters. **I,** Pseudotemporal ordering of NK single cell transcriptomes with Slingshot. Expression of selected genes alone the pseudotime. **J,** Volcano plot of differentially expressed genes between *Il27ra*$^{-/-}$ and *Il27ra*$^{+/-}$ NK clusters from tumors; upregulated in *Il27ra*$^{-/-}$ (red), downregulated (blue). **K,** Slingshot trajectory analysis for ILC1 cells. **L,** Normalized cell numbers representing upregulated and downregulated clusters among ILC1 cells in *Il27ra*$^{-/-}$ versus *Il27ra*$^{+/-}$. **M,** Pseudotemporal ordering of ILC1 single cell transcriptomes with Slingshot. Expression of selected genes along the pseudotime. **N,** Volcano plot of differentially expressed genes between tumor *Il27ra*$^{-/-}$ and *Il27ra*$^{+/-}$ ILC1 clusters; upregulated in *Il27ra*$^{-/-}$ (red), downregulated (blue). **O,** KEGG pathway analysis of differentially expressed genes along the trajectory of ILC1 clusters.

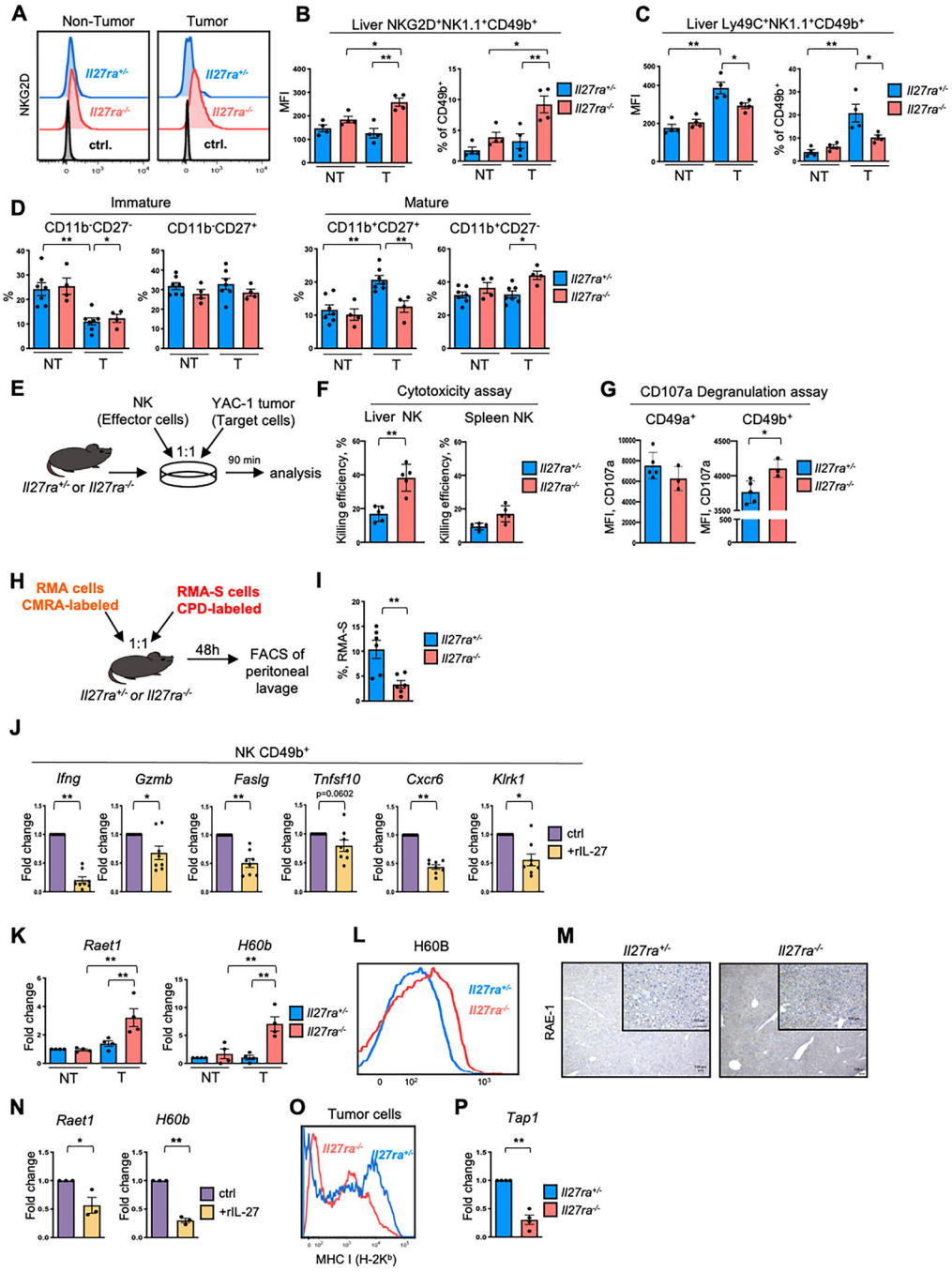

Figure 4. IL-27R signaling regulates NK cell activation and cytotoxicity.

A, Representative histogram of FACS analysis for NKG2D activating receptor expression. Mean fluorescence intensity (MFI) and percentage of NKG2D$^+$ **(B)** and Ly49C$^+$ **(C)** cells among CD49b$^+$ NK1.1$^+$ NK cells in non-tumor and tumor tissue from DEN-injected *Il27ra*$^{+/-}$ and *Il27ra*$^{-/-}$ mice (n=4). **D,** Single cell suspensions of non-tumor (NT) and tumor (T) tissue from DEN-injected *Il27ra*$^{+/-}$ (n=7) and *Il27ra*$^{-/-}$ mice (n=4) were analyzed by FACS. Percentage of immature (CD11b$^-$CD27$^-$ and CD11b$^-$CD27$^+$) and mature (CD11b$^+$CD27$^+$ and CD11b$^+$CD27$^-$) cells among NK1.1$^+$TCRβ$^-$ NK cells. **E,** Scheme for

cytotoxicity and degranulation assays. **F,** Cytotoxic activity of liver and splenic NK cells sorted by negative selection from *Il27ra*$^{+/-}$ (n=5) and *Il27ra*$^{-/-}$ (n=5) and co-cultured with target cancer cells. Percentage of dead target cells is shown. **G,** FACS analysis for surface CD107a as a marker of degranulation on sorted liver CD49a^{+} (ILC1) and CD49b^{+} (NK) cells from *Il27ra*$^{+/-}$ (n=5) and *Il27ra*$^{-/-}$ (n=3) mice, which were co-cultured with target cells. **H,** Scheme for *in vivo* cytotoxicity experiment. RMA-S (sensitive to NK killing) and RMA (insensitive) cell lines were dye-labelled, mixed in 1:1 ratio and injected i.p. into 8-week-old *Il27ra*$^{+/-}$ and *Il27ra*$^{-/-}$ mice; cell recovery was analyzed 48h later. **I,** Percentage of RMA-S cells from peritoneal lavage of *Il27ra*$^{+/-}$ (n=6) and *Il27ra*$^{-/-}$ (n=6) mice. **J,** Q-RT-PCR analysis of relative gene expression of NK cell related genes in CD49b^{+} NK cells sorted by magnetic bead positive selection from liver of wild type mice (n=8) and stimulated *in vitro* with rIL27. Gene expression was first normalized to *Rpl32,* then to gene expression in untreated conditions. **K,** Relative gene expression of stress molecules *Raet1* and *H60b* in NT and T tissues from DEN-injected *Il27ra*$^{+/-}$ and *Il27ra*$^{-/-}$ mice (n=4). **L,** FACS analysis and representative histogram of H60B expression on CD45-negative cells from tumors of *Il27ra*$^{+/-}$ and *Il27ra*$^{-/-}$ mice. **M,** Representative images of IHC RAE-1 staining of tumor-bearing livers of DEN-injected *Il27ra*$^{+/-}$ and *Il27ra*$^{-/-}$ mice. **N,** Relative gene expression (Q-RT-PCR) of *Raet1* and *H60b* in DEN-derived HCC cells treated *in vitro* with rIL27 (normalized to *Rpl32* and then to gene expression in untreated conditions). **O,** FACS analysis of MHCI/H-2K^{b} expression on CD45-negative cells from tumors of DEN-injected *Il27ra*$^{+/-}$ and *Il27ra*$^{-/-}$ 10-month-old mice. **P,** Relative gene expression (Q-RT-PCR; normalized to *Rpl32* and then to expression in tumor tissue of *Il27ra*$^{+/-}$ mice) of *Tap1* gene in tumor tissue of *Il27ra*$^{+/-}$ and *Il27ra*$^{-/-}$ mice (n=4). Data are mean ± SEM from at least 3 independent experiments. Tukey's multiple comparisons test **(D)**; *p<0.05. **p<0.01, unpaired Student's t-test (two-tailed).

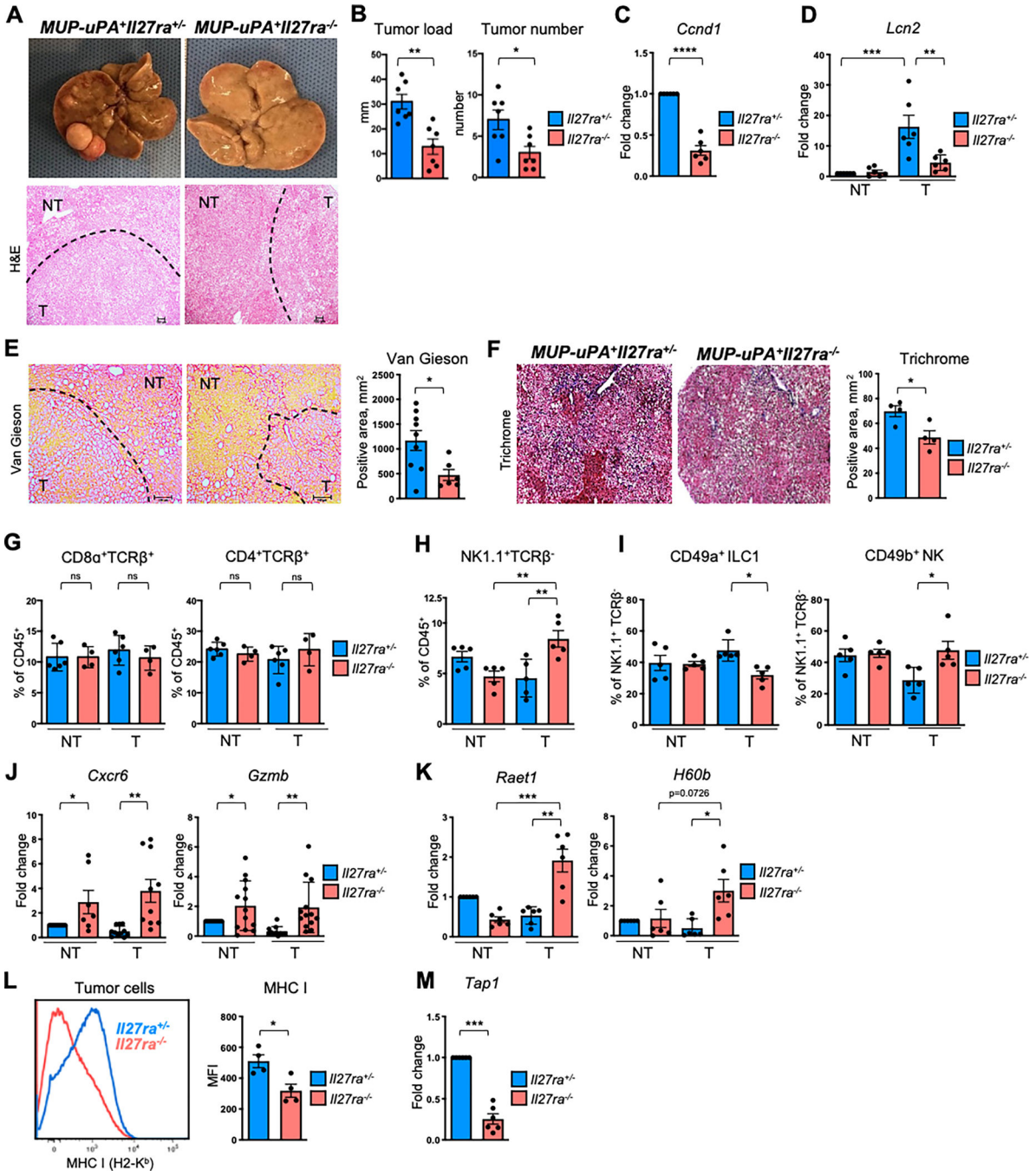

Figure 5. IL-27R signaling promotes tumor growth in NASH-driven HCC.

8-week-old *MUP-uPA*$^{+}$*Il27ra*$^{-/-}$ and *MUP-uPA*$^{+}$*Il27ra*$^{+/-}$ control mice were fed with a WD for 8 months. **A,** Representative macroscopic and microscopic (H&E staining) images of livers with tumors. **B,** Tumor load and tumor number of *MUP-uPA*$^{+}$*Il27ra*$^{+/-}$ (n=7) and *MUP-uPA*$^{+}$*Il27ra*$^{-/-}$ (n=7) male mice. Q-RT-PCR analysis of relative gene expression of *Ccnd1* **(C)** and *Lcn2* **(D)** in non-tumor (NT) and tumor (T) tissue from *MUP-uPA*$^{+}$ *l27ra*$^{+/-}$ (n=6) and *MUP-uPA*$^{+}$*Il27ra*$^{-/-}$ (n=6) male mice. **E,F,** Histological analysis and quantification of collagen content determined by Van Gieson **(E)** or Trichrome **(F)** staining

of liver sections from *MUP-uPA*$^{+}$*Il27ra*$^{+/-}$ and *MUP-uPA*$^{+}$*Il27ra*$^{-/-}$ male mice. **G-I,** FACS analysis of CD45^{+} immune cells in NT and T tissue of *MUP-uPA*$^{+}$*Il27ra*$^{+/-}$ and *MUP-uPA*$^{+}$*Il27ra*$^{-/-}$ mice. **G,** Percentage of CD8α^{+}TCRβ^{+} and CD4^{+}TCRβ^{+} cells among CD45^{+} populations. **H** and **I**, Percentage of NK1.1^{+}TCR β^{+} **(H)** and CD49a^{+} NK1.1^{+} and CD49b^{+} NK1.1^{+} **(I)** cells among CD45^{+} populations in NT and T tissues of *MUP-uPA*$^{+}$*Il27ra*$^{+/-}$ and *MUP-uPA*$^{+}$*Il27ra*$^{-/-}$ mice (n=4–6). **J ,K,** Q-RT-PCR analysis of relative gene expression of *Cxcr6*, *Gzmb* **(J)** and *Raet1*, *H60b* **(K)** in NT and T tissues from *MUP-uPA*$^{+}$*Il27ra*$^{+/-}$ and *MUP-uPA*$^{+}$*Il27ra*$^{-/-}$ mice (n=6–13). **L,** FACS analysis of MHC I expression on CD45^{-}CD31^{-}TER119^{-} tumor cells from *MUP-uPA*$^{+}$*Il27ra*$^{+/-}$ and *MUP-uPA*$^{+}$*Il27ra*$^{-/-}$ mice (n=4). Representative histogram and MFI of expression are presented. **M,** Q-RT-PCR analysis of relative gene expression of *Tap1* in tumors from *MUP-uPA*$^{+}$*Il27ra*$^{+/-}$ and *MUP-uPA*$^{+}$*Il27ra*$^{-/-}$ female and male mice (n=6). **C, M,** Gene expression was first normalized to *Rpl32* then to that in tumor tissue from *MUP-uPA*$^{+}$*Il27ra*$^{+/-}$ mice. **D,J,K,** Gene expression was first normalized to *Rpl32* then to gene expression in non-tumor tissue of *MUP-uPA*$^{+}$*Il27ra*$^{+/-}$ mice. Data are mean ± SEM from at least 3 independent experiments. *p<0.05. **p<0.01, ***p<0.001, unpaired Student's t-test (two-tailed); Tukey's multiple comparisons test.

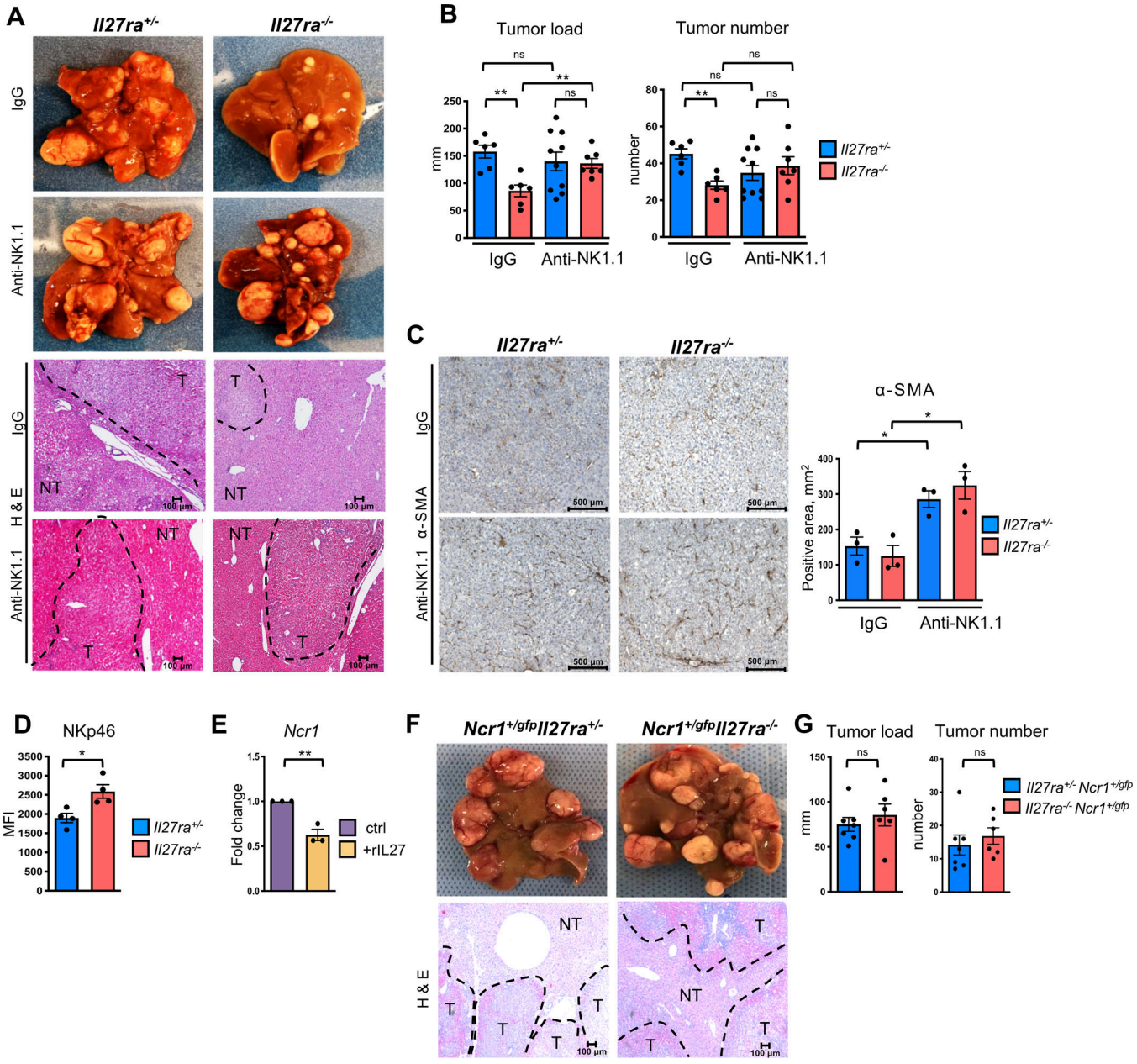

Figure 6. IL-27R signaling exerts its action via innate cytotoxic lymphocytes.

DEN-treated *Il27ra*$^{+/-}$ and *Il27ra*$^{-/-}$ mice were administered with anti-NK1.1 or IgG isotype control antibodies for 5.5 months prior to tumor development analysis at 10 months. **A,** Representative images of macroscopic and microscopic view of tumor-bearing livers. **B,** Tumor load and tumor number in IgG treatment group: *Il27ra*$^{+/-}$ (n=6), *Il27ra*$^{-/-}$ (n=6) and anti-NK1.1 treatment group: *Il27ra*$^{+/-}$ (n=10), *Il27ra*$^{-/-}$(n=7) mice. **C,** Representative images and quantification of α-SMA staining of HCC sections from DEN-treated *Il27ra*$^{+/-}$ (n=3) and *Il27ra*$^{-/-}$ (n=3) mice injected with anti-NK1.1 antibody or isotype control. **D,** Mean fluorescence intensity (MFI) of NKp46 surface expression on NK1.1^{+}TCRβ^{-} cells from livers of *Il27ra*$^{+/-}$ and *Il27ra*$^{-/-}$ mice as determined by FACS (n=4). **E,** Q-RT-PCR analysis of *Ncr1 (NKp46)* gene expression in CD49b^{+} NK cells purified from spleens of WT

naïve mice and stimulated *in vitro* with rIL27 (n=3). Gene expression was first normalized to *Rpl32* then to gene expression in untreated condition. **F,** Representative images of macroscopic view of tumor-bearing livers from $Ncr1^{+/gfp}Il27ra^{+/-}$ and $Ncr1^{+/gfp}Il27ra^{-/-}$ DEN-treated mice analyzed at 10 months of age. **G,** Tumor load and tumor number among $Ncr1^{+/gfp}Il27ra^{+/-}$ (n=7) and $Ncr1^{+/gfp}Il27ra^{-/-}$ (n=6) mice compared to $Il27ra^{+/-}$ (n=15) and $Il27ra^{-/-}$ (n=12) mice from the cohorts shown on Figure 1K. Data are mean ± SEM from at least 3 independent experiments. *p<0.05, **p<0.01, unpaired Student's t-test (two-tailed).

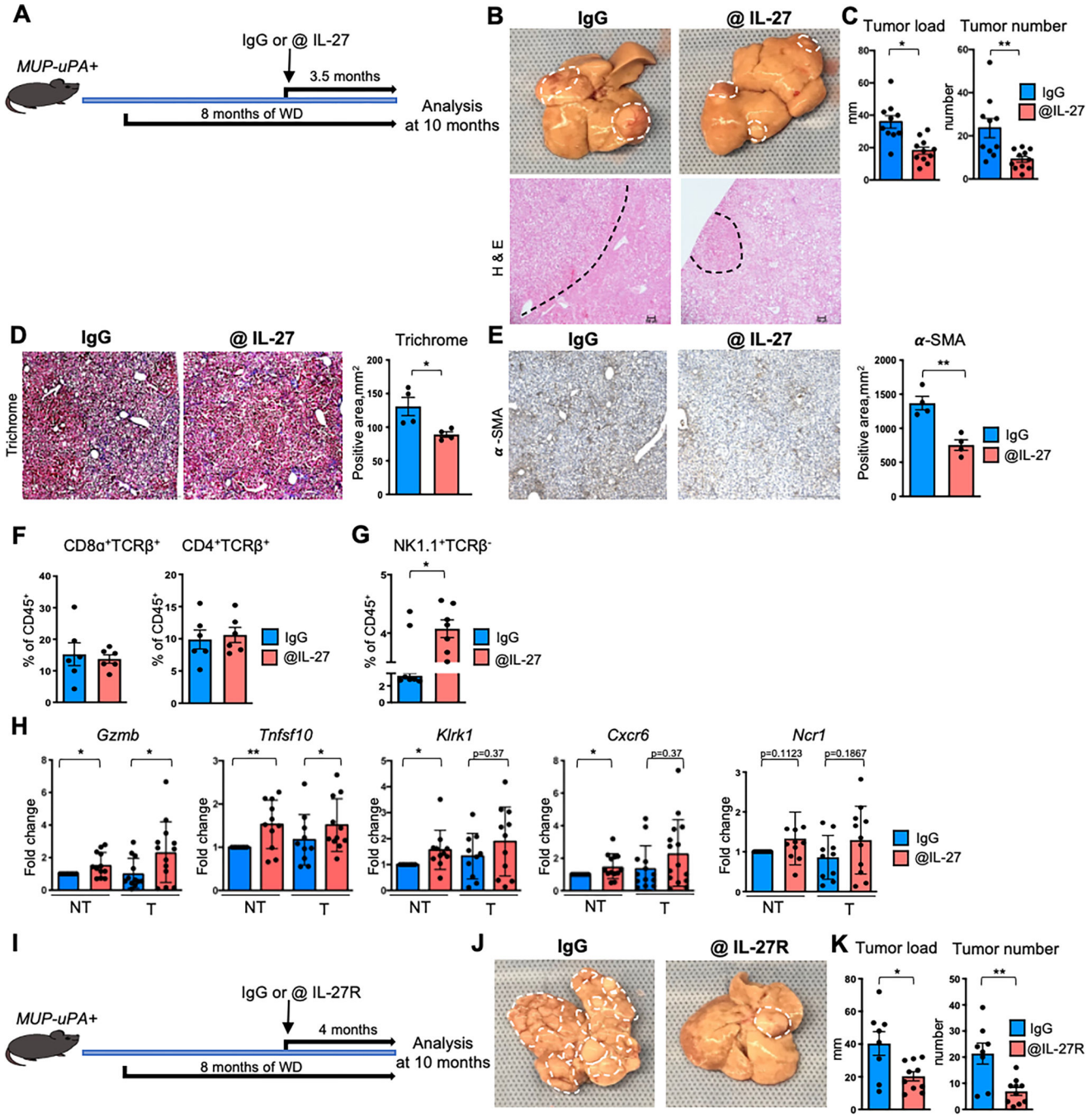

Figure 7. Pharmacologic blockade of IL-27 or IL-27R suppresses HCC tumor growth in NASH model.

A, 8-week-old *MUP-uPA*$^{+}$ mice were fed a WD for 8 months and received IgG or anti-IL-27 (SRF381) for 3.5 months prior to assessment of tumor development at 10 months. **B,** Representative images of macroscopic and microscopic view of tumor bearing livers. **C,** Tumor load and tumor number of IgG isotype control (n=10) and anti-IL-27 (n=11) treated mice. Representative images and quantification of fibrosis (collagen content) as determined by Trichrome staining **(D)** and α-SMA staining **(E)** of liver sections from *MUP-uPA*$^{+}$

mice that received *IgG* isotype control (n=4) or anti-IL-27 (n=4) treatment. Single cell suspensions of livers from mice that received IgG isotype control (n=6–7) or anti-IL-27 (n=6–7) treatment were analyzed by FACS. Percentage of $CD4^{+}TCR\beta^{+}$ and $CD8\alpha^{+}TCR\beta^{+}$ cells **(F)** and $NK1.1^{+}TCR\ \beta^{-}$ cells **(G)** among $CD45^{+}$ populations is presented. **H,** Q-RT-PCR analysis of relative gene expression of *Gzmb, Tnfsf10, Klrk1, Cxcr6* and *Ncr1* in NT and T tissue from IgG (n=10–15) and anti-IL-27 (n=10–17) mice. **I,** 8-week-old *MUP-uPA*$^{+}$ mice were fed a WD for 8 months and received IgG or anti-IL-27R for 4 months prior to assessment of tumor development at 10 months. **J,** Representative macroscopic images of livers with developed tumors. **K,** Tumor load and tumor number of IgG group (n=8) and anti-IL-27R (n=10) mice. Data are mean ± SEM from at least 3 independent experiments. *p<0.05. **p<0.01, ***p<0.001, unpaired Student's t-test (two-tailed).